Dorsal Motor Vagal Neurons Can Elicit Bradycardia and Reduce Anxiety-Like Behavior

Misty M. Strain[1]*, Nicholas J. Conley[2]*, Lily S. Kauffman[2]*, Liliana Espinoza[1], Stephanie Fedorchak[1], Patricia Castro Martinez[3], Maisie E. Crook[2], Maira Jalil[2], Georgia E. Hodes[4], Stephen B. G. Abbott[5], Ali D. Güler[2], John N. Campbell[2#] and Carie R. Boychuk[1,6#]

**co-first authors*
[#] co-corresponding authors

[1] Department of Cellular and Integrative Physiology, Long School of Medicine, University of Texas Health San Antonio, San Antonio, TX
[2] Department of Biology, University of Virginia, Charlottesville, VA
[3] Neuroscience Undergraduate Major, University of Virginia, Charlottesville, VA
[4] School of Neuroscience, Virginia Polytechnic Institute and State University, Blacksburg, VA
[5] Department of Pharmacology, University of Virginia, Charlottesville, VA
[6] Dalton Cardiovascular Research Center, University of Missouri, Columbia, MO

Running Title: Activating DMV reduces HR and anxiety.

Correspondence to:
Carie R. Boychuk, Ph.D. (lead contact)
Dalton Cardiovascular Research Center
Department of Biomedical Sciences
University of Missouri
College of Veterinary Medicine
1500 Research Park Drive
Columbia, Missouri 65203, USA
Telephone: 210-450-8449
Fax: 210-567-4410
Email: boychukc@missouri.edu

John N. Campbell, Ph.D.
Department of Biology
University of Virginia
485 McCormick Road
PO BOX 400328
Charlottesville, VA 22903, USA
Email: jnc4e@virginia.edu

Keywords: autonomic regulation, parasympathetic nervous system
Number of pages: 30
Number of figures: 4
Number of words in Abstract: 142

Number of words in Body: 4514
Total words: 7556
References: 63

SUMMARY:

Cardiovagal neurons (CVNs) innervate cardiac ganglia through the vagus nerve to control cardiac function. Although the cardioinhibitory role of CVNs in nucleus ambiguus (CVN^{NA}) is well established, the nature and functionality of CVNs in dorsal motor nucleus of the vagus (CVN^{DMV}) is less clear. We therefore aimed to characterize CVN^{DMV} anatomically, physiologically, and functionally. Optogenetically activating cholinergic DMV neurons resulted in robust bradycardia through peripheral muscarinic (parasympathetic) and nicotinic (ganglionic) acetylcholine receptors, but not beta-1-adrenergic (sympathetic) receptors. Retrograde tracing from the cardiac fat pad labeled CVN^{NA} and CVN^{DMV} through the vagus nerve. Using whole cell patch clamp, CVN^{DMV} demonstrated greater hyperexcitability and spontaneous action potential firing *ex vivo* despite similar resting membrane potentials, compared to CVN^{NA}. Chemogenetically activating DMV also caused significant bradycardia with a correlated reduction in anxiety-like behavior. Thus, DMV contains uniquely hyperexcitable CVNs capable of cardioinhibition and robust anxiolysis.

INTRODUCTION:

Cardiovagal neurons (CVNs) send axonal projections from hindbrain to cardiac ganglia through the vagus nerve to elicit cardioinhibitory (i.e., slowing of heart rate; HR) action at rest and during critical cardiorespiratory homeostatic reflexes. Although in mammals most CVNs are found in the nucleus ambiguus (CVN^{NA}), 20% of CVNs arise from a second region, the dorsal motor nucleus of the vagus (CVN^{DMV}) (Corbett et al., 1999; Hsieh et al., 1998; Izzo et al., 1993; Massari et al., 1995; Standish et al., 1994; Ter Horst et al., 1996). While the ability of CVN^{NA} to control chronotropy (e.g. HR) is well characterized (Geis and Wurster, 1980; Gilbey et al., 1984; McAllen and Spyer, 1977), whether this ability extends to CVN^{DMV} remains controversial, despite their extensive innervation of cardiac tissue (Cheng et al., 1999). CVN^{DMV} innervate cardiac tissue with unmyelinated, C fibers (Ford et al., 1990), the selective activation of which causes a bradycardia (or a decrease in HR) in multiple mammalian species (Jones et al., 1995; Nosaka et al., 1979). In addition, studies of CVN ontogenesis implicate DMV, not NA, as the primary vagal nucleus in lower-order vertebrates and in early mammalian embryonic development, since CVN^{NA} migrate out of DMV (Taylor et al., 2014; Taylor et al., 2022), making it possible that CVN^{DMV} retain functional cardioinhibitory activity in mammals.

Despite these anatomical studies, functional studies remain conflicting. Some argue that direct electrical stimulation of DMV does not change chronotropy (Geis and Wurster, 1980; Laughton and Powley, 1987), while others demonstrate local activation (chemical, electrical, optogenetic, or chemogenetic) elicits bradycardias even if only modestly (Falvey et al., 2023; Machhada et al., 2020; Machhada et al., 2016; Sporton et al., 1991; Thompson et al., 2023). However, no activation technique in awake animals

used to date rules out incidental stimulation of either neighboring nucleus tractus solitarius (NTS) neurons or inhibitory interneurons within DMV. Stimulation of this latter population could significantly dampen the impact of cholinergic premotor neuron stimulation. Thus, whether cholinergic CVN^{DMV} are capable of controlling chronotropy remains an important but open question.

A recent resurgence of interest in understanding of vagal physiology is driven by the growing number of therapeutic applications for vagus nerve stimulation (Ottaviani et al., 2022). Of particular interest, vagus nerve stimulation is a promising treatment for anxiety and post-traumatic stress disorder (Groves and Brown, 2005; Shivaswamy et al., 2022). In rats, stimulating the vagus nerve accelerates extinction of conditioned fear (Pena et al., 2013; Souza et al., 2022) and decreases anxiety-like behavior in the elevated plus maze paradigm (Shivaswamy et al., 2022). In humans, vagal nerve stimulation may even reduce treatment-resistant anxiety disorders (George et al., 2008). However, the mechanism behind the anxiolytic effect of vagal stimulation is currently unknown. Since the vagus nerve is a bidirectional nerve, carrying sensory information from viscera to brain and motor information from brain to viscera, the extent to which the anxiolytic effect of vagus nerve stimulation depends on sensory or motor signaling is unclear. One possibility is that activating the vagus nerve decreases anxiety by slowing HR, in line with the James-Lange theory of emotions (Lange and James, 1967). Accordingly, a recent study in mice demonstrated that tachycardia (e.g. increase in HR) is sufficient to induce anxiety-like behavior (Hsueh et al., 2023).

Controversy over the role of CVN^{DMV} may stem in part from differences in CVN^{NA} and CVN^{DMV} electrophysiology and thus their roles in regulating HR. Notably, CVN^{NA} are

largely quiescent *in vivo* and *ex vivo* (McAllen and Spyer, 1978; Mendelowitz, 1996), responding solely to integrated synaptic signaling. While limited data exist on the electrophysiological properties of CVN^{DMV} specifically, other DMV neuronal populations have unique pace-making properties and maintain a relatively high activity *ex vivo* (Browning et al., 1999), which allows for more complex signal processing. One investigation into their activity also suggests that, unlike CVN^{NA}, CVN^{DMV} do not demonstrate robust respiratory burst patterning (Jones et al., 1998). Therefore, it is tempting to speculate that CVN^{DMV} integrate and communicate central information differently from CVN^{NA} and represent a functionally unique circuit with respect to CVN^{NA}, which is consistent with evidence that CVN^{DMV} and CVN^{NA} target different cardiac ganglia (Cheng et al., 2004). A more extensive characterization of the electrophysiological properties of CVN^{DMV} will help build a foundation for understanding their cardioregulatory role, and importantly, for harnessing the therapeutic potential of vagus nerve stimulation. This is critical given that synaptic input to CVN^{DMV} is uniquely sensitive to perturbation of the cardiovascular system, relative to CVN^{NA} (Cauley et al., 2015).

The aim of the present study was to characterize the ability of DMV neurons to regulate HR functionally, physiologically, and pharmacologically. We hypothesized that activating choline acetyltransferase positive (Chat+) CVN^{DMV} elicits robust bradycardias. Moreover, we sought to characterize the electrophysiological properties of CVN^{DMV} to determine whether they are distinct from the more extensively studied CVN^{NA}. Testing of these hypotheses was accomplished using a combination of opto- and chemogenetic stimulation specifically in Chat+ neurons, pharmacology techniques to determine the regulatory role of CVN^{DMV} on chronotropy, and retrograde labeling paired with

electrophysiology procedures to examine differences between the two CVN populations. Our results raise the possibility that CVN^{DMV} play a role distinct from CVN^{NA} in regulating HR.

RESULTS

Optogenetic stimulation of Chat+ DMV can elicit bradycardia: To determine if CVN^{DMV} activation is capable of cardioinhibition, we used optogenetics to activate cholinergic neurons in DMV. Specifically, we crossed Ai32 mice expressing channelrhodopsin-2/EYFP fusion protein (ChR2) to loxP floxed choline acetyltransferase ($Chat^{cre}$) mice to selectively express ChR2 in Chat+ neurons ($Chat^{cre}$;ChR2). Male $Chat^{cre}$;ChR2 and $Chat^{cre}$ mice (Figure 1A) were implanted with HR telemetry devices and fiber optic probes above the right DMV and HR was examined before and during photostimulation. A preliminary study examined HR responses to 5 (-58 ± 28 bpm), 10 (-126 ± 26 bpm), 20 (-261 ± 32 bpm) and 40 (-43 ± 16 bpm) Hz stimulation to DMV in $Chat^{cre}$;ChR2 mice and found that 20 Hz elicited a significantly larger bradycardia compared to all other frequencies ($F(3,12) = 14.35$, $p = 0.0003$, n = 4; data not shown). We further verified that DMV neurons were continuously activated by 20 Hz photostimulation using whole cell patch clamp in brain slices from $Chat^{cre}$;ChR2 mice (Before: 2.9 ± 1.8 Hz versus During: 15.0 ± 2.4 Hz; $t(3) = 3.825$, $p = 0.03$; Figure 1B).

Photostimulating DMV in awake $Chat^{cre}$;ChR2 mice significantly decreased HR (280 ± 23 bpm) compared to $Chat^{cre}$;ChR2 HR before stimulation (606 ± 32 bpm, $p < 0.0001$, n = 9 mice; Figure 1E,F). Photostimulation failed to significantly affect HR in control, $Chat^{cre}$ mice (Before: 597 ± 61 bpm versus During: 611 ± 22 bpm, n = 4; p =

0.9720), confirming that photostimulation-induced bradycardia in Chat^{cre};ChR2 was not a consequence of off-target effects or exposure to a laser (e.g., tissue necrosis, light diffusion, temperature effects). Finally, photostimulation-induced bradycardia in Chat^{cre};ChR2 was significantly different from HR responses to light in Chat^{cre} control. All Fs > 17.11; $p < 0.0017$).

In contrast to photoexcitation of DMV neurons, photoinhibition of cholinergic neurons in DMV of awake mice using Chat^{cre} mice crossed to Ai39 mice conditionally expressing halorhodopsin (NpHR^{EYFP}), produced no significant HR response to light (Before: 629 ± 45 bpm versus During: 627 ± 38 bpm), t (2) = 0.1494, p = 0.8950, n=3). These results suggest that under these conditions DMV neurons are sufficient to regulate HR but not necessary for control of resting HR.

Since the axons of CVN^{NA} travel dorsally to converge with axons from CVN^{DMV} before turning and exiting the brainstem (e.g., McGovern and Mazzone, 2010), it was possible that cardioinhibitory actions of DMV resulted from stimulating nearby CVN^{NA} axons. To rule out CVN^{NA} axonal stimulation, we first examined c-Fos expression in ChAT+ neurons two hours post-DMV stimulation (Figure 1D). Qualitatively robust c-Fos was seen on the stimulated (right) side of DMV with no c-Fos expression in NA. We also confirmed using immunofluorescence that stimulating NA directly causes c-Fos expression (Figure 1K). Finally in a subset of anesthetized Chat^{cre};ChR2 mice, photostimulation of the exposed vagus nerve produced no change in HR (Before: 422 ± 61 bpm versus During: 419 ± 60 bmp; n = 3; $t(4) = 0.04$, $p = 0.9723$). Taken together, axonal expression of ChR2 in NA was not sufficient to activate NA and elicit bradycardia.

DMV photostimulation-induced bradycardia works through canonical vagal circuits: To confirm that DMV photostimulation affects HR though autonomic pathways, Chat^{cre};ChR2 mice were administered an *i.p.* injection of hexamethonium to block all nicotinic acetylcholine receptor (nAChR) communication between preganglionic and cardiac-projecting postganglionic parasympathetic neurons prior to DMV (n = 4) or NA (n = 3) photostimulation. Initial photostimulation of DMV (-261 ± 32 bpm) and NA (-255 ± 32 bpm) produced a similar robust bradycardia (p = 0.9931). As expected, pretreatment of hexamethonium abolished all photostimulation-induced bradycardia in both DMV and NA (3 ± 3 bpm and -2 ± 1, respectively, $F(1, 5) = 134.50$, $p < 0.0001$, Figure 1I-J*).*

To confirm that DMV photostimulation affects HR though muscarinic acetylcholine receptor (mAChR) activation from postganglionic parasympathetic neurons to cardiac tissue, consistent with canonical cardiovagal signaling, Chat^{cre};ChR2 mice received i.p. injections of scopolamine methylbromide (to block parasympathetic activity) and atenolol (to block sympathetic activity) in a randomized order prior to photostimulation (Figure 1G). In this subset of mice (n = 5), optogenetic activation of DMV neurons again induced robust bradycardia (-405 ± 46 bpm). While administration of atenolol modestly reduced DMV light-induced bradycardias (-276 ± 39 bpm, p = 0.003, Figure 1H), administering scopolamine methylbromide abolished it (14 ± 3 bpm, p = 0.002, Figure 1H, $F(1.166, 4.664) = 65.68$, p = 0.0006). Thus, both nAChR and mAChR activity is required for photostimulation-induced decreases HR from DMV similar to the NA. Some reports have suggested that DMV-mediated vagal activity on cardiac tissue occurs through non-canonical nicotinic nAChR communication between postganglionic parasympathetic neurons to cardiac tissue (Gee et al., 2023), However, our results confirm that no

bradycardia can be elicited after mAChR antagonism, providing strong evidence that DMV neurons induce robust bradycardia through nAChR→mAChR signaling (and not nAChR→nAChR), the canonical cardiovagal pathway.

DMV innervates cardiac tissue through the vagus nerve: Retrograde tracing with rhodamine and cholera toxin subunit B (CT-B) was done in male C57BL6/J mice to calculate the number of CVN^{DMV} and CVN^{NA} labeled by each tracer (n=6-8 mice per tracer for each CVN group; Figure 2A, B). Although both tracers identified positive neurons in NA and DMV, there were fewer traced neurons in CVN^{DMV} (31 ± 19) compared to CVN^{NA} (99 ± 16; $F(1, 22) = 23.70$, $p < 0.0001$; Figure 2C). In addition, CT-B (47 ± 36) labeled significantly fewer neurons than rhodamine regardless of region (83 ± 33; $F(1, 22) = 6.35$, $p = 0.0195$). There was not a significant interaction between CVN location and tracer, $F(1, 22) = 0.048$, $p = 0.8294$. To confirm that retrograde labeling of CVN^{DMV} required an intact vagus nerve, a unilateral left vagotomy prior to cardiac injection of rhodamine was performed in a separate group of animals (n = 3, Figure 2D). Unilateral vagotomy eliminated labeling of CVN^{DMV} ipsilateral to vagotomy (2 ± 1 labeled CVN^{DMV}) compared to the contralateral side (32 ± 8 labeled CVN^{DMV}, $t(2) = 4.38$, $p = 0.0483$; Figure 2E). Taken together, DMV contains neurons that retrogradely label from cardiac tissue in a vagus-dependent manner.

CVN^{DMV} show spontaneous firing and have larger input resistance *ex vivo* compared to CVN^{NA}: To characterize the electrophysiological properties of CVN^{DMV} in relation to CVN^{NA}, additional studies examined the general excitability of CVNs in male C57BL6/J mice using whole-cell patch-clamp electrophysiology under current clamp configuration. Retrogradely labeled CVNs were identified using visual inspection for

rhodamine and anatomical landmarks (Figure 3A). Post-hoc biocytin recovery confirmed location and cholinergic phenotype (Figure 3B). CVN^{DMV} exhibited more spontaneous firing (8/14 neurons from 10 mice) compared to CVN^{NA} (0/10 neurons from 9 mice, Fisher's exact test, $p = 0.0064$), which were completely devoid of any spontaneous firing activity (Figure 3C-D). Of CVN^{DMV} exhibiting spontaneous firing (57%), the average frequency was 1.28 ± 0.31 Hz.

No statistical differences in resting membrane potential were found between CVN^{DMV} (-58.60 ± 2.72 mV, n = 14 neurons from 10 mice) and CVN^{NA} (-62.18 ± 1.75 mV, n = 10 neurons from 9 mice, $t(22) = 1.01$, $p = 0.3256$, Figure 3E). However, we found that CVN^{DMV} (492.00 ± 22.02 MΩ, n = 14 neurons from 10 mice) demonstrated significantly larger input resistance (R_{input}) than CVN^{NA} (158.20 ± 10.61 MΩ, n = 10 neurons from 9 mice, $t(22) = 12.06$, $p < 0.0001$, Figure 3F-H).

CVN^{DMV} are hyperexcitable compared to CVN^{NA} *ex vivo*: To determine if there were any differences in excitability between CVN^{DMV} and CVN^{NA}, CVNs were examined for general excitability through stepped depolarizations of current (Figure 3I). As expected, regardless of neuronal type, stepped current injections evoked a current dependent increase in action potential frequency, $F(5, 108) = 85.01$, $p < 0.0001$ (Figure 3J). Additionally, a significant effect of neuronal type regardless of current injection was found, with CVN^{DMV} exhibiting a significantly greater number of evoked action potentials (5 ± 1 number of action potentials, n = 14) compared to CVN^{NA} (2 ± 1 number of action potentials, n = 10; $F(1, 22) = 23.40$, $p < 0.0001$). Finally, we found a significant interaction between current injection and neuronal type, with significantly more evoked action potentials in CVN^{DMV} compared to the CVN^{NA} at 100 (0.30 vs. 3.42 ± 0.5), 150 (0.80 vs.

5.00 ± 0.5), 200 (2.10 vs. 5.93 ± 0.5), and 250 pA (3.80 vs. 6.43 ± 0.6); $F(5, 108) = 6.72$, $p < 0.0001$ (Figure 3J). Taken together, CVN^{DMV} are more excitable than CVN^{NA}.

Chemogenetic activation of DMV suppresses HR for up to 8 hours: Although our optogenetic studies could rule out interneuron activity, they could not rule out off target stimulation of nearby Chat+ neurons (e.g., hypoglossal neurons) affecting HR. Therefore, to further confirm that activating DMV neurons specifically decreases HR, we used an alternative strategy, chemogenetically activating DMV neurons with the excitatory designer receptor, hM3Dq. Here, hM3Dq was specifically targeted to DMV neurons using an intersectional genetics approach which leverages the co-expression of *Chat* and *Phox2b* genes by DMV neurons but not by neighboring neurons (i.e., hypoglossal) (Kang et al., 2007; Tao et al., 2021). First, to validate this intersectional approach, $Chat^{Cre}$;$Phox2b^{Flp}$ mice were crossed with $R26^{ds\text{-}HTB}$ mice, a reporter line which expresses nuclear-localized, green fluorescent protein (GFP)-tagged histone 2b protein (H2b-GFP) upon recombination by both Cre and Flp. In the resulting $Chat^{Cre}$;$Phox2b^{Flp}$;$R26^{ds\text{-}HTB}$ mice, essentially all peripherally-projecting DMV neurons, as labeled by a systemic (i.p.) retrograde tracer, Fluorogold, were H2b-GFP immunofluorescent (136 of 139, 97.8%, Fluorogold+ DMV neurons were also H2b-GFP+; n=4 mice; representative image in Supplemental Figure 1A). These results confirm that $Chat^{Cre}$ and $Phox2b^{Flp}$ are co-expressed by all DMV vagal efferent neurons and thus validate our intersectional approach.

Next, to express hM3Dq specifically in DMV neurons, an adeno-associated virus (AAV) in which Cre- and Flp- dependently expresses a hemagglutinin (HA)-tagged hM3Dq (AAV1-CreON/FlpON-hM3Dq-HA; Figure 4A) was injected into DMV of male and

female Chat^{Cre};Phox2b^{Flp};R26$^{ds\text{-}HTB}$ mice. This resulted in hM3Dq-HA expression in the vast majority of H2b-GFP+ DMV neurons ("DMV-hM3Dq" mice; Figures 4A-C). Importantly, we failed to detect any hM3Dq-HA expression in NA (Figure 4B-C) or DMV of mice lacking Cre and Flp recombinases (Supplemental Figure 1B), confirming the specificity of our injection strategy and AAV expression.

To determine whether chemogenetically activating DMV neurons affects HR, hM3Dq ligand clozapine N-oxide (CNO; 1 mg/kg; i.p.) was administered while measuring HR by non-invasive electrocardiography (ECG; n=8 mice per genotype). Administering CNO to DMV-hM3Dq mice significantly decreased HR for up to 8 hours compared to baseline (baseline: 718 ± 10 bpm; 20 min: 497 ± 34 bpm, p = 0.0012; 40 min: 497 ± 30 bpm, p = 0.0008; 60 min: 467 ± 36 bpm, p = 0.0007; 2hr: 469 ± 39 bpm, p = 0.0011; 6hr: 598 ± 19 bpm, p = 0.0006; 8hr: 637 ± 24 bpm, p = 0.0274; F(1.833, 14.67) = 29.13, Figure 4D), though HR returned to baseline by 24 hours post-CNO (24hr: 731 ± 9 bpm, p = 0.7247). As expected, the acute bradycardia after CNO administration required peripheral muscarinic signaling, as it was abolished by administering the peripheral muscarinic blocker, methyl-atropine, 20min after CNO (baseline, 747 ± 5 bpm; after CNO, 640 ± 19 bpm, p = 0.0078 *vs*. baseline; after atropine, 801 ± 4 bpm, F(1.124, 7.869) = 43.88, p = 0.0004 *vs*. baseline; Figure 4E). On the other hand, administering CNO to hM3Dq-negative control mice failed to significantly alter HR (p>0.05 *vs*. baseline or vehicle; Figure 4E; Supplemental Figure 1C), indicating that CNO alone did not affect HR. These results, together with our optogenetics studies, provide robust evidence that DMV neurons can decrease heart rate through peripheral muscarinic signaling.

Activating DMV neurons reduces anxiety-like behavior: Tachycardia increases anxiety-like behavior in mice (Hsueh et al., 2023), consistent with the James-Lange theory that physiological cues can drive emotional states (Lange and James, 1967). Anecdotally, DMV-hM3Dq mice after CNO treatment were easier to handle, leading to questions about whether their CNO-induced bradycardia was associated with any change in anxiety-like behavior. To investigate, DMV-hM3Dq mice and control mice (n=8 per group) were again administered CNO but this time were assessed behaviorally by elevated plus maze, an assay for anxiety-like behavior (Figure 4F). Strikingly, compared to vehicle, CNO treatment in DMV-hM3Dq mice significantly increased their time spent in the open arms of the elevated plus maze (CNO, 16.9 ± 4.83 s; vehicle, 0.23 ± 0.23 s; $F(1.098,7.688)= 9.471$, $p = 0.0235$, Figure 4H). However, CNO had no such effect in control mice lacking hM3Dq, indicating that CNO alone did not affect open arm time (Supplemental Figure 1D). CNO treatment also significantly increased other indicators of anxiolysis in DMV-hM3Dq mice: time spent moving (CNO, 162.6 ± 14.4 s; saline, 40.7 ± 8.7 s; $F(1.720,12.04)=22.84$, $p = 0.0006$, Figure 4G); head dip events (CNO, 4.149 ± 1.022 dips; saline, 0.2414 ± 0.1424 dips; $F(1.024,6.146)=13.80$, $p = 0.0259$; Supplemental Figure 1E); and average velocity (CNO, 2.339 ± 0.3068 cm/s; saline, 0.6606 ± 0.2317 s, $F(1.482,8.894)=26.13$, $p = 0.0011$; Supplemental Figure 1F). These effects of CNO were largely abolished by co-administering methyl-atropine (“CNO+MA"), indicating that the anxiolytic effects, as with HR, require peripheral mAChR signaling (Figure 4G,H; Supplemental Figure 1D,E). Specifically, compared to vehicle treatment, CNO+MA failed to significantly affect open arm time, time spent moving, velocity or head dip events, relative to treatment with a saline vehicle ($p < 0.05$; Figure 4G,H,

Supplemental Figure 1D,E). In addition, CNO's effects on HR and open-arm time in DMV-hM3Dq mice were moderately correlated (r = 0.6394). Thus, activating DMV neurons causes a correlated reduction in HR and anxiety-like behavior through peripheral mAChR signaling.

DISCUSSION

The present study characterized CVN^{DMV} anatomically, physiologically, and functionally. Retrograde tracing from the cardiac fat pad confirmed the presence of CVN in DMV using two different tracers, rhodamine and CTB, and this labeling required an intact vagus nerve. Electrophysiological comparison of retrogradely-labeled CVN^{DMV} and CVN^{NA} indicate distinct circuits, with CVN^{DMV} being significantly more excitable with higher input resistances and spontaneous activity *ex vivo* whereas CVN^{NA} were not. Optogenetically activating DMV neurons caused bradycardia, which was completely abolished by muscarinic and nicotinic antagonism. Finally, intersectional chemogenetic activation of DMV neurons also caused bradycardia and a correlated decrease in anxiety-like behavior, both of which also required peripheral muscarinic signaling, as they were blocked by muscarinic antagonism.

Previous efforts to characterize *in vivo* electrophysiological properties of DMV neurons are limited, possibly a result of their prominent C-fiber phenotypes and long latency conduction times (Jones et al., 1998) making typical antidromic spike identification challenging. Our retrograde labeling findings are in accordance with previous reports, which suggest that only ~20% of CVN exist within DMV in totality (both sides), making the likelihood of recording from these numbers *in vivo* relatively low (Taylor et al., 2014).

Importantly, CVNs signal organization is an established example of divergent amplification, meaning that changes in HR arise from modulation (activation or inhibition) of a relatively small number of CVNs (McAllen and Spyer, 1978). Therefore, whole-cell patch-clamp recordings paired with retrograde labeling in adult animals—albeit confounded by the absence of relevant synaptic inputs *in vivo*—is a powerful technique that future studies should continue to use to aid in the investigation of this population of neurons both in health and disease.

Our *ex vivo* results are consistent with electrophysiological recording in other DMV populations. DMV neurons demonstrate an on-going activity phenotype (Browning et al.; Travagli and Gillis, 1994; Travagli et al., 1991). This was true in the present study as ~57% of CVN^{DMV} demonstrated a spontaneously active firing pattern during the recording period. With regards to CVNs, this on-going firing activity is unique to CVN^{DMV} since no CVN^{NA} recorded exhibited any spontaneous activity in our slice preparation, which is also consistent with previous results from CVN^{NA} (Mendelowitz, 1996). While future studies will need to demonstrate how this spontaneous activity is generated, it is consistent with the intrinsic pace-making properties of other DMV neurons. However, it also suggests that CVN^{DMV} may represent a functionally discrete circuit for cardiac-related vagal motor output. Previous studies suggest that CVN^{DMV} have little respiratory-related burst activity, despite robust lung-related afferent activity (Jones et al., 1998), which is in contrast to the CVN^{NA} which show robust respiratory-related burst activity both *in vivo* and *ex vivo* (McAllen and Spyer, 1977). While we are only beginning to elucidate the complexity of vagal circuits as it relates to any vagal motor output, there is increasing evidence for distinct circuits related to vagal sensory afferents. Similar distinct circuits also likely exist

in vagal motor nuclei (Coverdell et al., 2022; Tao et al., 2021; Veerakumar et al., 2022). While some parallel circuits have converging anatomy and function, they may be distinct in terms of their physiological roles (Veerakumar et al., 2022). Finally, CVN^{DMV} demonstrates a significantly higher input resistance and higher number of spiking activity to current injections compared to CVN^{NA}. Therefore, CVN^{DMV} are more excitable than CVN^{NA}. In other brain regions, this type of behavior confers a coincidence detection phenotype over a simple integrator (Konig et al., 1996). Therefore, future work should continue to investigate how CVNs in NA and DMV differ in their microcircuit construction in relation to the basic circuit building blocks of critical homeostatic regulating networks.

Despite historical controversy about the capacity of CVN^{DMV} to impact HR, our results demonstrate that optogenetic and chemogenetic activation of Chat+ DMV neurons each caused robust bradycardia (~56% and ~65.5% of resting HR, respectively) in awake, behaving mice. Cardioinhibitory responses using optogenetic techniques in urethane-anesthetized rats and ketamine/xylazine-anesthetized mice demonstrated variable strength of the response (Machhada et al., 2020; Thompson et al.), implicating differences in anesthesia for differences in effect size. Alternatively, previous species used (namely cats and rats) may exhibit a lesser degree of DMV-activation driven bradycardia than mice because of differences in vagal tonus. Since mice have a lower vagal tone than rats for example (Carnevali and Sgoifo, 2014; Marmerstein et al., 2021; Swoap et al., 2004), CVN^{DMV} activation in mice may recruit a larger number of CVN^{DMV} which were not previously active. However, optogenetic inhibition of DMV in mice failed to change HR, similar to previous reports using chemogenetic receptors (Machhada et al., 2016). While this latter result suggests CVN^{DMV} activity may not be necessary for

generation of resting HR, the present study introduced a significant refinement of techniques using Chat^{cre} mice to eliminate the impact of known interneurons within DMV.

While this refinement eliminates the influence of interneurons within DMV, the anatomical proximity of vagal axons from NA and the optrode in DMV (Taylor et al., 2014) raises the possibility that DMV stimulation resulted in axonal stimulation of CVN^{NA} neurons. However, we failed to detect c-Fos expression in NA and DMV contralateral to the optoprobe, despite robust c-Fos immunoreactivity in the ipsilateral DMV. In addition, direct stimulation of the vagus nerve bundle in Chat^{cre};ChR2 animals did not produce photostimulation-induced bradycardia. Finally, the more restricted genetic targeting using chemogenetic activation did not label near-by cholinergic regions, including NA or hypoglossal while causing similar cardioinhibition as DMV stimulation in Chat^{cre};ChR2. Taken together, these data provide robust evidence that DMV activation and not NA axonal stimulation or interneuron activation results in cardioinhibition (Figure 1D).

As expected, pharmacological testing confirmed that DMV stimulation requires muscarinic ACh receptor activation in mice, since scopolamine (but not atenolol) and methyl-atropine abolished optogenetically- and chemogenetically-induced bradycardia, respectively. Notably, while the traditional concept of vagal motor signaling to cardiac tissue requires nicotinic receptor-dependent communication between preganglionic and postganglionic parasympathetic neurons, some studies report that intracardiac ganglia harvested from SA node also show muscarinic ACh receptor-dependent neurotransmitter and calcium mobilization (Beker et al., 2003). Additional studies have attributed pharmacological differences in vagal fiber activation to C-fiber (presumably from DMV) versus B-fiber bradycardia (presumably from NA) since hexamethonium did not block the

HR responses to non-myelinated fiber activation in these studies (Ford and McWilliam, 1986). Still, it is important to note that the aforementioned studies did not comment on whether postganglionic neurons were isolated from cardiac nodal cells, nor did they directly address the effect of neurotransmitter release on the observed HR responses. Our findings are in accordance with the canonical signaling pathway between preganglionic and postganglionic parasympathetic neurons, as pre-treatment with the nicotinic ACh receptor antagonist, hexamethonium, completely abolished light-induced bradycardia in ChAT^{cre};ChR2 mice.

Recent research suggests that HR can influence emotional states, supporting a theory of emotion separately proposed by the physiologist Carl Lange and psychologist William James over a century ago. As explained by James: "*My thesis […] is that the bodily changes follow directly the Perception of the exciting fact, and that our feeling of the same changes as they occur IS the emotion."* (James, 1884). In other words, the James-Lange theory holds that HR does not increase because of anxiety; rather, the perception of HR increase is the anxiety. Consistent with this theory, a recent study in mice demonstrated that optogenetically increasing HR is sufficient to drive anxiety-like behaviors in the elevated plus maze (Hsueh et al., 2023). Inversely, beta-blockers such as propranolol, which robustly decrease HR (Black et al., 1964), also reduce anxiety-like behaviors in mice (Gorman and Dunn, 1993; Wohleb et al., 2011). Beta-blockers and other drugs which decrease heart rate have shown promise for treating anxiety and related disorders (Repova et al., 2022). Studies of brain activity in humans and mice suggest the insular cortex may play a key role in sensing HR and other interoceptive cues (Critchley et al., 2004; Hassanpour et al., 2018; Hsueh et al., 2023; Khalsa et al., 2009)

and so could couple the perception of heart rate to emotional state. Importantly, however, while our study is the first to our knowledge to demonstrate a correlation between vagally-mediated bradycardia and anxiolysis, more research is needed to establish a causal relationship. Whether other physiological functions of DMV, such as gut motility, glucose metabolism, and suppressing inflammation (Coverdell et al., 2023), can influence anxiety-like behavior remains unknown. In any case, a decrease in anxiety is the most likely explanation for the increases in overall movement and exploratory behavior that we observed.

In summary, this study demonstrates the existence of CVN^{DMV} neurons and their ability to suppress HR and anxiety-like behavior. The cardioinhibitory and behavioral effects both require muscarinic Ach receptor activity, and our results also suggest that nicotinic Ach receptors are involved in the signaling between CVN^{DMV} and cardiac parasympathetic neurons, implicating canonical vagal pathways in DMV's facilitation of cardioinhibitory activity. CVN^{DMV} also has distinct electrophysiological properties, namely spontaneous firing activity and higher R_{input}, compared to CVN^{NA} *in slice*. Therefore, we further speculate that CVN^{DMV} represents a unique population of CVNs, distinct from the more thoroughly characterized CVN^{NA}. Further research is needed to identify the molecular profile of CVN^{DMV}, the mechanisms underlying their distinct electrophysiological properties, and their physiological role.

ACKNOWLEDGEMENTS: Funding was provided by a Pathway to Stop Diabetes Initiator Award 1-18-INI-14, an NIH R01 HL153916 to J.N.C., an NIH R01HL157366 to C.R.B. and an NIH T32 HL007446 for M.M.S.

AUTHOR CONTRIBUTIONS. M.M.S., N.J.C., L.S.K., M.J., S.B.G.A., J.N.C., and C.R.B. designed experiments. L.E., S.F., and M.M.S performed optogenetic and cardiac tracing studies, including HR analysis, and all histology/immunofluorescence. L.E. and C.R.B. performed electrophysiological studies. A question from G.E.H. inspired the study of anxiety-like behavior. N.J.C., L.S.K., M.E.C., and P.C.M. performed chemogenetic study of HR and anxiety-like behavior. N.J.C. and L.S.K. performed histology and immunofluorescence experiments related to chemogenetic studies. N.J.C., J.N.C., M.M.S., L.E., and C.R.B. prepared figures. M.M.S, N.J.C., L.S.K., C.R.B., and J.N.C. wrote the manuscript with input from all authors.

DECLARATION OF INTEREST

Authors declare no competing interest.

FIGURE CAPTIONS:

Figure 1: Optogenetic stimulation of DMV elicits bradycardia. Genetic crossbreeding paradigm used to generate transgenic mice harboring loxP-flanked ChR2 in Chat-positive motor neurons (A). Photostimulation-evoked action potentials from DMV motor neurons pace to 20 Hz stimulation (B). Representative diagram illustrating confirmed locations of optogenetic probes (C). Representative images of DMV (top) and NA (bottom) stained for the neuronal activation marker, c-Fos (middle panel; red) and GFP (left panel; green) immunoreactivity confirming c-Fos activation in DMV, but not NA, after DMV photostimulation (D). Representative traceI) and mean HR (F) showing optogenetic

stimulation of DMV produced a bradycardia in mice expressing $Chat^{cre}$;ChR2 but not in $Chat^{cre}$ mice. Representative trace (G) and mean HR (H) showing muscarinic parasympathetic blocker, methyl-scopolamine, eliminated the photostimulation-induced bradycardia, while sympathetic blockage with β-1 receptor blocker atenolol mildly reduced this bradycardia. Representative images of probe site (top) and immunohistochemical staining of NA showing c-Fos activation after stimulation of NA (K). Representative trace (I) and mean HR (J) showing the nicotinic antagonist, hexamethonium abolished photostimulation-induced bradycardia in both DMV and NA. Bars represent mean and SEM. Blue bars/shading indicates light stimulation. *Indicates significance $p \leq 0.05$.

Figure 2: DMV innervates cardiac tissue through the vagus nerve in male mice. Schematic showing injection into the epicardial fat pad and labeling in both CVN brain regions (A). Representative images of DMV and NA after cardiac injection of retrograde tracers, rhodamine (left in red) and cholera toxin subunit B (CT-B; right in green) (B). Both rhodamine and CT-B significantly labeled cardiac projecting neurons in NA and DMV (C). Representative images of DMV after a right cervical vagotomy (C). Representative image (D) and mean cell count (E) showing a right cervical vagotomy significantly attenuated CVN^{DMV} numbers ipsilateral to vagotomy. Bars represent mean and SEM. *Indicates significance $p \leq 0.05$.

Figure 3: Differential electrophysiological properties of CVN^{DMV} compared to CVN^{NA} in male mice. Rhodamine-positive DMV neurons showing pipette (top) and rhodamine

(bottom; red) (A). Representative immunofluorescence image of CVN^{DMV} showing biocytin recovered patched cardiac-labeled neurons are cholinergic (B). Representative trace (C) and mean firing rate (D) of CVN^{DMV} neurons show significantly higher spontaneous firing rates compared to CVN^{NA}, with the majority of CVN^{DMV} firing. No statistical differences in resting membrane potential were found between CVN^{DMV} and CVN^{NA} (E). Representative traces of membrane responses from CVN^{NA} (top) and CVN^{DMV} (bottom) to stepped current injections (F). Current-voltage (I-V) relationship graph obtained from CVN^{NA} and CVN^{DMV} (G). R_{input} was higher in CVNDMV compared to CVNNA (H). Representative action potential responses in CVNNA (top) and CVNDMV (bottom) in response to 300 pA injection of direct depolarizing current (I). Action potential response curves were higher in CVNDMV compared to CVNNA in response to 50 pA-step injections of direct depolarizing current (J). * Indicates significance $p \leq 0.05$.

Figure 4: Chemogenetic stimulation of DMV produces bradycardia and reduces anxiety. Illustration of coronal hindbrain section showing injection site and *Chat* and *Phox2b* expression (A, top left); Schematic of AAV1-CreON/FlpON-hM3Dq-HA viral construct (A, bottom); Venn diagram showing expected expression of hM3Dq-HA and H2b-GFP (A, top right). (B). Representative images of rostral, intermediate, caudal DMV and NA stained for HA (magenta) and H2b-GFP (green) immunoreactivity in $Chat^{Cre}$;$Phox2b^{Flp}$;$R26^{ds\text{-}HTB}$ mice after DMV injection of AAV1-CreON/FlpON-hM3Dq-HA. (C). Percentage of H2b-GFP+ cells immunoreactive for hM3Dq-HA in the rostral, intermediate and caudal DMV and NA. (D). Effect of CNO on heart rate (HR) in DMV-hM3Dq mice over 24-hour period. CNO 1mg/kg (i.p.*)* at time = 0 min. (E). Effect of saline, CNO and CNO+MA on HR in

DMV-hM3Dq (magenta) and control mice (black); comparisons are to baseline. (F). Schematic of elevated plus maze (EPM) experiment. (G). Effects of saline vehicle, CNO and CNO+MA administration (i.p.) on time spent moving in the elevated plus maze, in seconds. (H). Effect of saline vehicle, CNO and CNO+MA administration (i.p.) on open arm time in the elevated plus maze, in seconds. (I). Correlation between changes in HR and open arm time between saline and CNO conditions in DMV-hM3Dq mice. *$p \leq 0.05$, **$p \leq 0.01$, ***$p \leq 0.001$, ****$p \leq 0.0001$.

Supplemental Figure 1: (A). Representative images of intermediate DMV hemisphere stained for H2b-GFP (green) and fluorogold immunoreactivity (blue) in $Chat^{Cre}$;$Phox2b^{Flp}$;$R26^{ds\text{-}HTB}$ mice after *(i.p.)* systemic injection of retrograde tracer Flurogold (136 of 139, 97.8%, Fluorogold+ DMV neurons were also H2b-GFP+); n=4 mice). (B). Representative images of intermediate DMV stained for HA (magenta) and H2b-GFP (green) immunoreactivity in $R26^{ds\text{-}HTB}$ mice (Cre-/Flp-) after DMV injection of AAV1-CreON/FlpON-hM3Dq-HA. (C). Effect of saline (white), CNO (magenta) and CNO+MA (green) on HR in DMV-hM3Dq and control mice; comparisons to vehicle. (D). Effect of saline or CNO on control mice, which lack hM3Dq expression, open arm time in the elevated plus maze, n=8 mice. (E-F) Effect of saline, CNO and CNO+MA in DMV-hM3Dq mice on head dip events and velocity in the elevated plus maze. *$p \leq 0.05$, **$p \leq 0.01$, ***$p \leq 0.001$, ****$p \leq 0.0001$.

REFERENCE:

Beker, F., Weber, M., Fink, R.H., and Adams, D.J. (2003). Muscarinic and nicotinic ACh receptor activation differentially mobilize Ca2+ in rat intracardiac ganglion neurons. J Neurophysiol *90*, 1956-1964.

Black, J.W., Crowther, A.F., Shanks, R.G., Smith, L.H., and Dornhorst, A.C. (1964). A New Adrenergic Betareceptor Antagonist. Lancet *1*, 1080-1081.

Browning, K.N., Renehan, W.E., and Travagli, R.A. (1999). Electrophysiological and morphological heterogeneity of rat dorsal vagal neurones which project to specific areas of the gastrointestinal tract. J Physiol *517 (Pt 2)*, 521-532.

Carnevali, L., and Sgoifo, A. (2014). Vagal modulation of resting heart rate in rats: the role of stress, psychosocial factors, and physical exercise. Front Physiol *5*, 118.

Cauley, E., Wang, X., Dyavanapalli, J., Sun, K., Garrott, K., Kuzmiak-Glancy, S., Kay, M.W., and Mendelowitz, D. (2015). Neurotransmission to parasympathetic cardiac vagal neurons in the brain stem is altered with left ventricular hypertrophy-induced heart failure. Am J Physiol Heart Circ Physiol *309*, H1281-1287.

Cheng, Z., Powley, T.L., Schwaber, J.S., and Doyle, F.J., 3rd (1999). Projections of the dorsal motor nucleus of the vagus to cardiac ganglia of rat atria: an anterograde tracing study. J Comp Neurol *410*, 320-341.

Cheng, Z., Zhang, H., Guo, S.Z., Wurster, R., and Gozal, D. (2004). Differential control over postganglionic neurons in rat cardiac ganglia by NA and DmnX neurons: anatomical evidence. Am J Physiol Regul Integr Comp Physiol *286*, R625-633.

Corbett, E.K., Batten, T.F., Kaye, J.C., Deuchars, J., and McWilliam, P.N. (1999). Labelling of rat vagal preganglionic neurones by carbocyanine dye DiI applied to the heart. Neuroreport *10*, 1177-1181.

Council., N.R. (2011). In Guide for the Care and Use of Laboratory Animals (Washington (DC): The National Academies Press).

Coverdell, T.C., Abbott, S.B.G., and Campbell, J.N. (2023). Molecular cell types as functional units of the efferent vagus nerve. Semin Cell Dev Biol.

Coverdell, T.C., Abraham-Fan, R.J., Wu, C., Abbott, S.B.G., and Campbell, J.N. (2022). Genetic encoding of an esophageal motor circuit. Cell Rep *39*, 110962.

Critchley, H.D., Wiens, S., Rotshtein, P., Ohman, A., and Dolan, R.J. (2004). Neural systems supporting interoceptive awareness. Nat Neurosci *7*, 189-195.

Daigle, T.L., Madisen, L., Hage, T.A., Valley, M.T., Knoblich, U., Larsen, R.S., Takeno, M.M., Huang, L., Gu, H., Larsen, R.*, et al.* (2018). A Suite of Transgenic Driver and

Reporter Mouse Lines with Enhanced Brain-Cell-Type Targeting and Functionality. Cell *174*, 465-480 e422.

Falvey, A., Palandira, S.P., Chavan, S.S., Brines, M., Tracey, K.J., and Pavlov, V.A. (2023). Electrical stimulation of the dorsal motor nucleus of the vagus regulates inflammation without affecting the heart rate. bioRxiv.

Ford, T.W., Bennett, J.A., Kidd, C., and McWilliam, P.N. (1990). Neurones in the dorsal motor vagal nucleus of the cat with non-myelinated axons projecting to the heart and lungs. Exp Physiol *75*, 459-473.

Ford, T.W., and McWilliam, P.N. (1986). The effects of electrical stimulation of myelinated and non-myelinated vagal fibres on heart rate in the rabbit. J Physiol *380*, 341-347.

Gee, M.M., Hornung, E., Gupta, S., Newton, A.J.H., Cheng, Z.J., Lytton, W.W., Lenhoff, A.M., Schwaber, J.S., and Vadigepalli, R. (2023). Unpacking the multimodal, multi-scale data of the fast and slow lanes of the cardiac vagus through computational modelling. Exp Physiol.

Geis, G.S., and Wurster, R.D. (1980). Cardiac responses during stimulation of the dorsal motor nucleus and nucleus ambiguus in the cat. Circ Res *46*, 606-611.

George, M.S., Ward, H.E., Jr., Ninan, P.T., Pollack, M., Nahas, Z., Anderson, B., Kose, S., Howland, R.H., Goodman, W.K., and Ballenger, J.C. (2008). A pilot study of vagus nerve stimulation (VNS) for treatment-resistant anxiety disorders. Brain Stimul *1*, 112-121.

Gilbey, M.P., Jordan, D., Richter, D.W., and Spyer, K.M. (1984). Synaptic mechanisms involved in the inspiratory modulation of vagal cardio-inhibitory neurones in the cat. J Physiol *356*, 65-78.

Gorman, A.L., and Dunn, A.J. (1993). Beta-adrenergic receptors are involved in stress-related behavioral changes. Pharmacol Biochem Behav *45*, 1-7.

Groves, D.A., and Brown, V.J. (2005). Vagal nerve stimulation: a review of its applications and potential mechanisms that mediate its clinical effects. Neurosci Biobehav Rev *29*, 493-500.

Hassanpour, M.S., Simmons, W.K., Feinstein, J.S., Luo, Q., Lapidus, R.C., Bodurka, J., Paulus, M.P., and Khalsa, S.S. (2018). The Insular Cortex Dynamically Maps Changes in Cardiorespiratory Interoception. Neuropsychopharmacology *43*, 426-434.

Hsieh, J.H., Chen, R.F., Wu, J.J., Yen, C.T., and Chai, C.Y. (1998). Vagal innervation of the gastrointestinal tract arises from dorsal motor nucleus while that of the heart largely from nucleus ambiguus in the cat. J Auton Nerv Syst *70*, 38-50.

Hsueh, B., Chen, R., Jo, Y., Tang, D., Raffiee, M., Kim, Y.S., Inoue, M., Randles, S., Ramakrishnan, C., Patel, S.*, et al.* (2023). Cardiogenic control of affective behavioural state. Nature *615*, 292-299.

Izzo, P.N., Deuchars, J., and Spyer, K.M. (1993). Localization of cardiac vagal preganglionic motoneurones in the rat: immunocytochemical evidence of synaptic inputs containing 5-hydroxytryptamine. J Comp Neurol *327*, 572-583.

James, W. (1884). What is an emotion? Mind *9*, 188-205.

Jones, J.F., Wang, Y., and Jordan, D. (1995). Heart rate responses to selective stimulation of cardiac vagal C fibres in anaesthetized cats, rats and rabbits. J Physiol *489 (Pt 1)*, 203-214.

Jones, J.F., Wang, Y., and Jordan, D. (1998). Activity of C fibre cardiac vagal efferents in anaesthetized cats and rats. J Physiol *507 (Pt 3)*, 869-880.

Kang, B.J., Chang, D.A., Mackay, D.D., West, G.H., Moreira, T.S., Takakura, A.C., Gwilt, J.M., Guyenet, P.G., and Stornetta, R.L. (2007). Central nervous system distribution of the transcription factor Phox2b in the adult rat. J Comp Neurol *503*, 627-641.

Khalsa, S.S., Rudrauf, D., Feinstein, J.S., and Tranel, D. (2009). The pathways of interoceptive awareness. Nat Neurosci *12*, 1494-1496.

Konig, P., Engel, A.K., and Singer, W. (1996). Integrator or coincidence detector? The role of the cortical neuron revisited. Trends Neurosci *19*, 130-137.

Lange, C.G., and James, W. (1967). The Emotions (New York,: Hafner Pub. Co.).

Laughton, W.B., and Powley, T.L. (1987). Localization of efferent function in the dorsal motor nucleus of the vagus. Am J Physiol *252*, R13-25.

Littlejohn, E.L., Espinoza, L., Lopez, M.M., Smith, B.N., and Boychuk, C.R. (2019). GABA(A) receptor currents in the dorsal motor nucleus of the vagus in females: influence of ovarian cycle and 5alpha-reductase inhibition. J Neurophysiol *122*, 2130-2141.

Machhada, A., Hosford, P.S., Dyson, A., Ackland, G.L., Mastitskaya, S., and Gourine, A.V. (2020). Optogenetic Stimulation of Vagal Efferent Activity Preserves Left Ventricular Function in Experimental Heart Failure. JACC Basic Transl Sci *5*, 799-810.

Machhada, A., Marina, N., Korsak, A., Stuckey, D.J., Lythgoe, M.F., and Gourine, A.V. (2016). Origins of the vagal drive controlling left ventricular contractility. J Physiol *594*, 4017-4030.

Marmerstein, J.T., McCallum, G.A., and Durand, D.M. (2021). Direct measurement of vagal tone in rats does not show correlation to HRV. Sci Rep *11*, 1210.

Massari, V.J., Johnson, T.A., and Gatti, P.J. (1995). Cardiotopic organization of the nucleus ambiguus? An anatomical and physiological analysis of neurons regulating atrioventricular conduction. Brain Res *679*, 227-240.

McAllen, R.M., and Spyer, K.M. (1977). Bradycardia produced by iontophoretic activation of preganglionic vagal motoneurones [proceedings]. J Physiol *269*, 49P.

McAllen, R.M., and Spyer, K.M. (1978). Two types of vagal preganglionic motoneurones projecting to the heart and lungs. J Physiol *282*, 353-364.

McGovern, A.E., and Mazzone, S.B. (2010). Characterization of the vagal motor neurons projecting to the Guinea pig airways and esophagus. Front Neurol *1*, 153.

Mendelowitz, D. (1996). Firing properties of identified parasympathetic cardiac neurons in nucleus ambiguus. Am J Physiol *271*, H2609-2614.

Nosaka, S., Yamamoto, T., and Yasunaga, K. (1979). Localization of vagal cardioinhibitory preganglionic neurons with rat brain stem. J Comp Neurol *186*, 79-92.

Ottaviani, M.M., Vallone, F., Micera, S., and Recchia, F.A. (2022). Closed-Loop Vagus Nerve Stimulation for the Treatment of Cardiovascular Diseases: State of the Art and Future Directions. Front Cardiovasc Med *9*, 866957.

Pena, D.F., Engineer, N.D., and McIntyre, C.K. (2013). Rapid remission of conditioned fear expression with extinction training paired with vagus nerve stimulation. Biol Psychiatry *73*, 1071-1077.

Repova, K., Aziriova, S., Krajcirovicova, K., and Simko, F. (2022). Cardiovascular therapeutics: A new potential for anxiety treatment? Med Res Rev *42*, 1202-1245.

Schneider, C.A., Rasband, W.S., and Eliceiri, K.W. (2012). NIH Image to ImageJ: 25 years of image analysis. Nat Methods *9*, 671-675.

Shivaswamy, T., Souza, R.R., Engineer, C.T., and McIntyre, C.K. (2022). Vagus Nerve Stimulation as a Treatment for Fear and Anxiety in Individuals with Autism Spectrum Disorder. J Psychiatr Brain Sci *7*.

Souza, R.R., Powers, M.B., Rennaker, R.L., McIntyre, C.K., Hays, S.A., and Kilgard, M.P. (2022). Timing of vagus nerve stimulation during fear extinction determines efficacy in a rat model of PTSD. Sci Rep *12*, 16526.

Sporton, S.C., Shepheard, S.L., Jordan, D., and Ramage, A.G. (1991). Microinjections of 5-HT1A agonists into the dorsal motor vagal nucleus produce a bradycardia in the atenolol-pretreated anaesthetized rat. Br J Pharmacol *104*, 466-470.

Standish, A., Enquist, L.W., and Schwaber, J.S. (1994). Innervation of the heart and its central medullary origin defined by viral tracing. Science *263*, 232-234.

Strain, M.M., Espinoza, L., Fedorchak, S., Littlejohn, E.L., Andrade, M.A., Toney, G.M., and Boychuk, C.R. (2023). Early central cardiovagal dysfunction after high fat diet in a murine model. Sci Rep *13*, 6550.

Swoap, S.J., Overton, J.M., and Garber, G. (2004). Effect of ambient temperature on cardiovascular parameters in rats and mice: a comparative approach. Am J Physiol Regul Integr Comp Physiol *287*, R391-396.

Tao, J., Campbell, J.N., Tsai, L.T., Wu, C., Liberles, S.D., and Lowell, B.B. (2021). Highly selective brain-to-gut communication via genetically defined vagus neurons. Neuron *109*, 2106-2115 e2104.

Taylor, E.W., Leite, C.A., Sartori, M.R., Wang, T., Abe, A.S., and Crossley, D.A., 2nd (2014). The phylogeny and ontogeny of autonomic control of the heart and cardiorespiratory interactions in vertebrates. J Exp Biol *217*, 690-703.

Taylor, E.W., Wang, T., and Leite, C.A.C. (2022). An overview of the phylogeny of cardiorespiratory control in vertebrates with some reflections on the 'Polyvagal Theory'. Biol Psychol *172*, 108382.

Ter Horst, G.J., Hautvast, R.W., De Jongste, M.J., and Korf, J. (1996). Neuroanatomy of cardiac activity-regulating circuitry: a transneuronal retrograde viral labelling study in the rat. Eur J Neurosci *8*, 2029-2041.

Thompson, D.A., Tsaava, T., Rishi, A., Nadella, S., Mishra, L., Tuveson, D.A., Pavlov, V.A., Brines, M., Tracey, K.J., and Chavan, S.S. (2023). Optogenetic stimulation of the brainstem dorsal motor nucleus ameliorates acute pancreatitis. Front Immunol *14*, 1166212.

Travagli, R.A., and Gillis, R.A. (1994). Hyperpolarization-activated currents, IH and IKIR, in rat dorsal motor nucleus of the vagus neurons in vitro. J Neurophysiol *71*, 1308-1317.

Travagli, R.A., Gillis, R.A., Rossiter, C.D., and Vicini, S. (1991). Glutamate and GABA-mediated synaptic currents in neurons of the rat dorsal motor nucleus of the vagus. Am J Physiol *260*, G531-536.

Veerakumar, A., Yung, A.R., Liu, Y., and Krasnow, M.A. (2022). Molecularly defined circuits for cardiovascular and cardiopulmonary control. Nature *606*, 739-746.

Wohleb, E.S., Hanke, M.L., Corona, A.W., Powell, N.D., Stiner, L.M., Bailey, M.T., Nelson, R.J., Godbout, J.P., and Sheridan, J.F. (2011). beta-Adrenergic receptor antagonism prevents anxiety-like behavior and microglial reactivity induced by repeated social defeat. J Neurosci *31*, 6277-6288.

LEAD CONTACT

Further information and requests for resources and reagents should be directed to and will be fulfilled by the lead contact, Carie R. Boychuk (BoychukC@missouri.edu).

MATERIALS AVAILABILITY

All data reported in this paper will be shared by the lead contact upon request. This study did not generate new unique reagents or report original code.

EXPERIMENTAL MODEL AND SUBJECT DETAILS

Mice: All animal procedures were approved by the Institutional Animal Care and Use Committee (IACUC) at the University of Texas Health San Antonio (UTHSA) or University of Virginia (UVA). Procedures were in accordance with the National Institutes of Health Guide for the Care and Use of Laboratory Animals (Council., 2011). All mice were maintained under standard conditions with access to food and water *ad libitum* on a 14:10 light cycle in a temperature regulated room (23.9 ± 1.7 °C) at the University of Texas Health San Antonio (UTHSA) or a 12:12 light cycle in a temperature regulated room (20.6 ± 1.9 °C) at the University of Virginia (UVA). Mice were randomly assigned to experimental groups and age-matched (9-52 weeks old). Animals were group housed unless stated otherwise. Sex is stated in the figure legends. All mice are maintained on a C57BL6/J background unless otherwise specified, and genotyping was performed according to guidelines from Jackson Laboratory or by Transnetyx. C57BL6/J adult mice were used for all experiments if not otherwise defined.

Optogenetic activation and HR: To generate a colony of transgenic mice with a constitutive knock-in of channelrhodopsin (ChR2) or halorhodopsin (NpHR) in cholinergic neurons ($Chat^{cre}$;ChR2 and $Chat^{cre}$;NpHR, respectively), mice harboring a Cre-dependent cation channel channelrhodopsin (ChR2; Ai32(RCL-ChR2(H134R)/EYFP; Jackson Laboratory, #024109) or halorhodopsin (NpHR; Ai39(RCL-eNpHR3.0/EYFP; Jackson Laboratory, #014539) were crossed with a $ChAT^{IRES\text{-}cre}$ mouse lines (B6.129S-$Chat^{tm1(cre)Lowl}$/MwarJ; Jackson Laboratory). This

breeding strategy generates mice expressing ChR2 or NpHR in Chat neurons ("Chat^{cre};ChR2" and "Chat^{cre};NpHR" mice, respectively; Figure 1A).

To provide specificity of activation to DMV or NA, Chat^{cre};ChR2, Chat^{cre};NpHR, or control (Chat$^{IRES\text{-}cre}$) mice were anesthetized with isoflurane to effect on a heating pad. Surgical sites were shaved and aseptically prepared with betadine and alcohol. Mice were first implanted with a heart rate telemetry (HRT) device (DSI, ETA-F10 implants, #270-0160-001) as previously detailed (Strain et al., 2023). Briefly, a vertical midline abdominal incision was made through the skin and peritoneal cavity. The telemetry device was placed in the peritoneal cavity with the leads tunneled to protrude from the peritoneal space. HR leads were then sutured in place in Lead II configuration and the peritoneal cavity closed with 4-0 silk suture. Wound clips were used to close the abdominal incision.

Following HRT implantation, mice were fixed in a stereotaxic frame (Kopf Instruments, Model 962) and an optical fiber cannula (Thorlabs, 0.50 NA, Ø200 µm Core Multimode Fiber, FP200URT) was inserted through a hole drilled through the skull just dorsal to the DMV (anterior/posterior: -7.43 mm, medial/lateral: 0.25 mm, dorsal/ventral: -2.65 mm) or NA (anterior/posterior: -7.31 mm, medial/lateral: 1.25 mm, dorsal/ventral: -3.95 mm). Optical fibers were secured using dental cement (A-M Systems, #525000 and 526000) and skull screws (Plastics One, 0-80- X 1/16). Subcutaneous administration of analgesics (buprenorphine 0.1 mg/kg and carprofen 10 mg/kg) were administered on the day of surgery and as needed for pain relief. Mice were monitored post-operatively for three days and allowed a week for recovery and acclimation to recording chambers.

During optogenetic stimulation trials, awake, behaving mice were temporarily singly housed with water available *ad libitum.* Photostimulation was performed using a diode-pumped solid state blue (for Chat^{cre};ChR2; 470 nm, Opto Engine LLC, MDL-III-470-300mW) or green laser (for Chat^{cre};NpHR; 532 nm; Opto EngineLLC, MGL-III-532-300mW). Optical matching gel (Zeiss, Immersol 518F) was applied at the ferrule junction to reduce light loss. Transmission efficiency of

all implanted lasers was confirmed prior to implantation (≥14 mW, 26.2 ± 6.8 mW) with a light meter (ThorLabs, PM100D). Phototrials consisted of 30 s of 20 Hz stimulation at 25mW pulsed laser output for DMV and 8mW for NA. All recordings occurred between 12:00 and 18:00 hour. Signals from HRT probes were acquired at a sampling frequency of 1 kHz using Spike 2 and DSI MX2 PhysioTel telemetry hardware (#48059). HR was acquired 30 s before photostimulation and during a 30 s photostimulation period using Spike 2 (version 9) software (Cambridge Electronic Design Limited). All probe placements were confirmed postmortem (Figure 1B).

For assessment of autonomic contributions to optogenetic stimulation, scopolamine methylbromide (1 mg/kg, Sigma Aldrich), a muscarinic acetylcholine receptor antagonist; atenolol (10 mg/kg, Sigma Aldrich), a β1 adrenergic receptor antagonist; and autonomic ganglionic blocker hexamethonium (30 mg/kg), a nicotinic ACh receptor (nAChR) antagonist, were injected intraperitoneally (i.p.). A minimum of 15 minutes was allotted after drug injection before optogenetic stimulation.

Optogenetic stimulation of the vagus nerve: Chat^{cre};ChR2 mice (10-20 weeks old; body weight, 31 ± 6g) were anesthetized with ketamine/xylazine (100 mg/kg; 10 mg/kg) and placed on a heating pad before the surgical site was shaved and aseptically prepared with betadine and alcohol. A five mm cervical incision was made at midline. Blunt dissection was used to isolate the right cervical vagus nerve from the carotid sheath. Mineral oil was applied to the exposed nerve to keep it moist. An optogenetic probe was placed one mm from the exposed vagus nerve. After a 15-minute acclimation period, the vagus nerve was stimulated for 20 s at 20 Hz at an intensity of 25 mW. A total of three simulations were done with a 5-minute inter-stimulation interval.

Retrograde Tracing: Mice were anesthetized with ketamine/xylazine (100 mg/kg; 10 mg/kg) and ventilated (CWE SAR-830/AP with mouse attachment 12-01020) in the supine position on a heating pad (37 ˚C). The surgical site was shaved and aseptically prepared with betadine and alcohol. A small (~5 mm) incision was made to access the thoracic cavity and the pericardial sac was incised. Cholera toxin subunit-b (recombinant) conjugated with Alexa Fluor

488 (CTB; 0.1 % v/v, 100 mM, Invitrogen) or tetramethylrhodamine-5-(and-6)-isothiocyanate conjugated with 5(6)-TRITC (rhodamine; 100 mL, Invitrogen T490) was then injected into the pericardial fat pad near the posterior right atrioventricular junction where cardiovagal nerve endings terminate. Surgical incisions were closed with 4-0 silk suture. Mice were monitored post-operatively for 3-6 days and allowed a week for recovery before experiments. Subcutaneous administration of analgesics (buprenorphine 0.1 mg/kg and carprofen 10 mg/kg) were administered on the day of surgery and as needed for pain relief.

Vagotomy: A subset of mice were anesthetized with ketamine/xylazine (100 mg/kg; 10 mg/kg) and ventilated (CWE SAR-830/AP, with mouse attachment 12-01020) in the supine position on a heating pad (37 ˚C). The surgical site was shaved and aseptically prepared with betadine and alcohol before a 5 mm cervical incision was made at midline. Blunt dissection was used to isolate the right cervical vagus nerve from the carotid sheath. A ~ 2 mm section was transected from the left cervical vagal nerve—sparing the aortic depressor nerve—to prevent regrowth/reattachment of the nerve. The superficial muscle and the cutaneous layer of the neck were sutured close with 4-0 silk suture. Mice then underwent retrograde tracing procedures as detailed above. Brains were harvested for immunohistochemistry procedures six days after retrograde tracing.

Electrophysiology: Mice (9-11 weeks old; 24.17 ± 0.86 g) were deeply anesthetized with isoflurane (3-4% in O_2) to effect (*i.e.*, lack of tail-pinch response) and decapitated while anesthetized. Brainstems were rapidly removed and immediately submerged in ice-cold (0–4°C) artificial cerebrospinal fluid (aCSF) equilibrated with carbogen gas (95% O_2, 5% CO_2). The aCSF composition (in mM) was: 124 NaCl, 3 KCl, 26 $NaHCO_3$, 1.4 NaH_2PO_4, 11 glucose, 1.3-2 $CaCl_2$, and 1.3 $MgCl_2$ (Littlejohn et al., 2019). Osmolarity of all solutions was 290–305 mOSM; pH = 7.3–7.4. Brainstems were mounted and 300 µm coronal slices containing DMV and NA were cut using a vibratome (Leica Biosystems). Slices were transferred to a holding chamber and incubated in warmed (32–34 °C) oxygenated aCSF containing 1mM kynurenic acid (kyn-aCSF) for 20 min.

Slices were then transferred to an oxygenated holding chamber at room temperature where they were maintained before being placed in a recording chamber mounted on a fixed stage of an upright microscope (BX51WI; Olympus), where they were continuously superfused again with warmed (32–34 °C), oxygenated aCSF (not containing kyn).

Whole-cell patch-clamp recordings under current clamp configuration were performed using infrared illumination and differential interference contrast optics (IR-DIC) under visual control. For recordings, glass pipettes (2–5 MΩ; King Precision Glass, Claremont, CA) were filled with a solution containing the following (in mM): 130 K+-gluconate, 1 NaCl, 5 EGTA, 10 HEPES, 1 $MgCl_2$, 1 $CaCl_2$, and Mg-ATP, pH titrated to 7.33-7.39 with KOH. Biocytin was added to the internal solution to identify patched neuron identity and location post-recording. Action potential (AP) frequency, resting membrane potential (RMP), and input resistance (R_{input}) were measured. RMP was corrected for liquid junction potential post hoc (−7 mV). R_{input} was measured by injecting 400 ms current pulse of -80 to +40 pA in 20 pA increments. To measure AP response to depolarizing current pulses (400 ms) of increasing amplitude (50 to 300 pA), background current was injected to maintain the membrane potential of patched neurons at approximately −60 mV to ensure a consistent starting voltage between current injection sweeps. Number of APs during each depolarizing current step were counted.

Recordings were discarded if series resistance was >25 MΩ or changed by >20% throughout the course of the experiment. Average series resistance was 9.64 ± 1.01 MΩ in the DMV and 11.71 ± 1.55 MΩ in the NA. Electrophysiological signals were acquired at 10 kHz and recorded using an Axoclamp 700B amplifier (Molecular Devices), low-pass filtered at 2 kHz, and stored to a computer using a Digidata 1440A digitizer and pClamp 10.2 software (Molecular Devices). For all electrophysiological experiments, data from only one cell per slice was included for data analysis. No more than three cells were used from one animal per region. A minimum of 8-10 min following establishment of whole-cell configuration was used to allow equilibration of the

intracellular recording pipette contents. Two min of continuous recording of steady-state activity was analyzed offline with Clampex 10.6 (Molecular Devices).

Chemogenetic activation: For chemogenetic studies, Chat^{Cre};Phox2b^{Flp};R26$^{ds\text{-}HTB}$ mice (13-52 weeks old; body weight, 25 ± 5g) were generated by first breeding Chat-Cre mice (Chat$^{tm1(cre)Lowl}$; JAX #028861) to Phox2b-Flp mice (Tg(Phox2b-flpo)3276Grds; JAX #022407), and then crossing the Chat^{Cre};Phox2b^{Flp} offspring to R26$^{ds\text{-}HTB}$ mice (gift of Martyn Goulding, Salk Institute for Biological Studies). The R26$^{ds\text{-}HTB}$ mouse line expresses a nuclear-localized, green fluorescent protein (GFP)-tagged histone 2b protein from the Rosa26 locus upon recombination by both Cre and Flp. Adult Chat^{Cre};Phox2b^{Flp};R26$^{ds\text{-}HTB}$ mice and R26$^{ds\text{-}HTB}$-only control mice were anesthetized with ketamine (80 mg/kg) and xylazine (10 mg/kg) then placed in a stereotaxic frame and on a servo-controlled heating pad to maintain a 37.0 ± 0.2 °C body temperature (RightTemp Jr.; Kent Scientific). Surgical sites were shaved and cleaned with betadine and isopropyl alcohol and injected with Nocita (long-lasting bupivacaine, 5.3 mg/kg, subcutaneously) for pre-operative analgesia. The dorsal surface of the medulla was then exposed by gently retracting the overlaying neck muscles and incising the meninges. A NanoJect III (Drummond Scientific, catalog #3-000-207) was used to inject 40nL of adeno-associated virus (AAV) Cre/Flp-dependently expressing hemagglutinin (HA)-tagged hM3Dq (AAV1-CreON/FlpON-hM3Dq-HA) at each of 8 injection sites (320nL total volume) to ensure infection throughout the DMV (from calamus scriptorius; anterior/posterior: ±0.3 mm, medial/lateral ±0.15 mm, dorsal/ventral: -0.25 and -0.5). Injections were made at 25nl/sec and 5 minutes were allowed between injections to minimize viral spread up the pipette track. After the final injection, the retracted muscles were sutured together over the injection site using absorbable sutures, and the skin was closed with vetbond surgical glue. Mice were provided with Meloxicam Sustained-Release (ZooPharm; 5mg/kg; IP) for post-operative analgesia, 1 mL of lactated Ringers solution in 5% dextrose to support hydration, and returned to the vivarium when ambulatory. After injecting their DMV with AAV1-CreON/FlpON-hM3Dq-HA, the Chat^{Cre};Phox2b^{Flp};R26$^{ds\text{-}HTB}$ mice are referred to as “DMV-hM3Dq” mice. Mice

were monitored post-operatively for five days and allowed to fully recover (three weeks) before acclimation to experimental environments and procedures.

Non-Invasive Electrocardiography: For 24-hour heart rate monitoring, mice were placed individually in portable electrocardiography (ECG) towers (ECGenie, Mouse Specifics Inc.) according to the manufacturer's instructions. ECG data were analyzed with EzCG software (Mouse Specifics, Inc.). After a 30 minute acclimation period, baseline HR measurements (-20 min timepoint) were obtained by averaging at least three 10 sec epochs, which were manually reviewed to exclude those containing motion artifacts. Mice were then intraperitoneally injected with clozapine N-oxide (CNO; 1.0mg/kg) at time 0. HR measurements from at least three 10 sec epochs were averaged per mouse per timepoint: 0 min; 20 min; 40 min; 60 min; 120 min; 6 hr; 8 hr; and 24 hr. Mice were kept in the towers from the -20 min timepoint until the 60 min timepoint, after which they were returned to their cages with access to food and water. For the 120 min, 6 hr, and 8 hr time points, mice were placed back into the towers for ECG recording and then returned to their cages. After the 8 hr time point, mice were returned to the vivarium. For the 24 hr timepoint, mice were re-acclimated for 30 min in the towers before collecting ECG data. Male and female mice were run on separate days.

For acute heart rate monitoring, mice were housed individually in ECGenie towers. As controls, we used CaTCh mice, a Cre/Flp reporter strain (Gt(ROSA)26Sor$^{tm80.1(CAG-COP4*L132C/EYFP)Hze}$, JAX # 025109, (Daigle et al., 2018)) on a (129S6/SvEvTac x C57BL/6NCrl) genetic background. Mice were acclimated to the towers for 30 min before recording baseline HR measurements. At 20 min intervals, mice were temporarily removed from the towers and administered each of the following injections (i.p) in the order listed: saline vehicle, CNO (1.0 mg/kg) and CNO plus methyl-atropine bromide (CNO+MA) (CNO, 1.0 mg/kg; MA, 1.0 mg/kg, Sigma Aldrich, catalog # 2870-71-5). For each mouse, the same volume of saline, CNO, and CNO+MA was injected. HR measurements were recorded 15 min after each injection and

averaged as described above. Other than temporary removal for injections, mice remained in the ECG towers for the duration of the experiment (approximately 1.5 hr).

Elevated Plus Maze: The elevated plus maze (EPM) is made of plexiglass and consists of four arms (two open without walls and two closed with walls) (Figure 4F). The maze sits approximately 0.6 meters above the floor, on a columnar platform, and underneath a video camera. The maze occupies a dedicated procedural room which is kept at constant temperature (66 °C) and illumination (100-120 lumens). Barriers are used so that the experimenter cannot be seen while the mouse is in the maze. All mice were acclimated to the experimenter and handling a minimum of 5 days prior to testing. Additionally, mice were acclimated to the behavioral room and maze for 3 training sessions prior to testing. DMV-hM3Dq mice (see above; n=8) and their controls (n=8) were randomly assigned to three groups and the order of the three treatments – saline vehicle, CNO 1.0mg/kg, and CNO+MA (CNO, 1.0 mg/kg; methy-atropine, MA, 1.0 mg/kg) - was randomized. The experimenter running the EPM test was blinded to treatment until after all treatments were complete. Just prior to testing, mice were acclimated to the behavior room for 30 min. Each mouse received one i.p. injection, either saline vehicle, CNO, or CNO+MA, 20 min prior to testing and was then gently placed into the closed arm of the maze. Mice are allowed free exploration of the maze for each 10 min session. Mouse movement was tracked over this 10 min period using a video camera and automated tracking software (Noldus, EthoVision). The time spent in open arms, time spent moving, velocity and head dip events are each calculated for the 10 min period using Noldus EthoVision software. Mice underwent each treatment condition twice, and results were averaged between the two trials. Mice were allowed at least 24 hours recovery between testing days. The maze was wiped clean with 70% ethanol spray before each use.

Immunohistochemistry: At the termination of electrophysiology experiments, brain slices were post-fixed with 4% PFA and then cryoprotected in 30% sucrose for at least two days before being sectioned (40 μM) on a cryostat at -19 ˚C. Biocytin-filled neurons were processed via avidin, Texas Red staining (TX Red Avidin D; 1:400; Vector Laboratories, A-2206). Free floating sections

were also immuno-labeled for ChAT to detect co-labeling of ChAT-positive motor neurons as detailed above.

At the termination of optogenetic experiments, mice were heavily anesthetized with isoflurane before transcardially perfusion with 0.1 M phosphate buffered saline (PBS) followed by 4% paraformaldehyde (PFA). Brains were cryoprotected in 30% sucrose before being sectioned (40 μm) on a cryostat at -19 ˚C (Leica Biosystems; CM 1860). Immunohistochemistry was performed on free floating sections for the immediate early gene product, cFos protein, as a marker of neuronal activation (rabbit anti-cFos, 1:1000, Synaptic Systems, 226 003), and ChAT to identify co-labeling of ChAT-positive motor neurons in DMV and NA. The following secondary antibodies were used: donkey-anti-rabbit (Alexa Fluor 488, 1:200, Invitrogen #A32790) and donkey-anti-goat (Alexa Fluor 568, 1:200, Invitrogen #A-11057). Negative controls were run without primary antibody.

At the termination of chemogenetic HR and behavioral studies, mice were transcardially perfused as described above. Brains were then cryoprotected in 25% sucrose solution before being sectioned (35 μm) on a freezing microtome (SM2010R, Leica Biosystems). Next, brain sections were washed 3 times for 5 minutes each in phosphate buffered saline (PBS) on a shaker. After washing, brain sections were incubated in blocking solution (PBS with 0.1% Triton X, PBT, plus 2% donkey serum) overnight at 4°C. Next, immunohistochemistry was performed on free floating sections for hemagglutinin (HA; reporter for hM3Dq expression) (chicken-anti-HA 1:200, catalog # ET-HA100, Aves Labs, Davis, CA) and ChAT (goat anti-ChAT, 1:250, catalog # AB144P, Sigma Aldrich, St. Louis, MO) on brain sections representing the rostral, mid, and caudal DMV. Primary antibodies were diluted in blocking solution and added to brain sections for 2 hours at room temperature. A second wash cycle (3 rounds of 5 min) with PBS is performed before transferring the brain sections to secondary antibody solution. The following secondary antibodies were used: donkey-anti-chicken (Alexa Fluor 647, 1:2000, Thermo Scientific #A78952) and donkey-anti-goat (Alexa Fluor 568, 1:200, Invitrogen, catalog # A-11057). All secondaries were

diluted in blocking solution and left to incubate overnight at room temperature. Following secondary incubation, brain sections underwent a third wash cycle (3 rounds of 5 min) in PBS before brain tissue was then mounted on glass slides, cover-slipped with a DAPI-containing mounting medium (Vectashield, H-1000, Vector Labs, Newark, CA), and imaged on a fluorescence microscope (Revolve, Echo, San Diego, CA) using filters suitable for the appropriate fluorescent dyes and the following objectives: Olympus 2x Apochromat PLAN APO 2X objective, numerical aperture (NA) 0.08, working distance (WD), 6.2mm; Olympus 10x Fluorite U PLAN PHASE FLUORITE 10X objective, Ph1 Phase, NA 0.30, WD 10mm; Olympus 20x Apochromat U PLAN S-APO 20X objective, NA 0.75, WD 0.6mm. Images were processed using Revolve Pro software and Image J (Schneider et al., 2012).

QUANTIFICATION AND STATISTICAL ANALYSIS

Results are reported as mean ± standard error of the mean (S.E.M.). Graph creation and statistical analysis was conducted in GraphPad Prism 9 (GraphPad Software). Specific statistical tests are noted in the Results. In general, two-tailed unpaired Student's *t* test was conducted with parametric data containing two groups. A Chi squared test was conducted with non-parametric data containing two groups. A one-way ANOVA followed by *Tukey's* multiple comparisons was used when there was one independent variable and more than two groups. A two-way ANOVA followed by *Šídák's* Multiple Comparison Test was used when there were two independent variables. Repeated-measures ANOVA was used when comparing multiple timepoints within subjects. The Geisser-Greenhouse correction was used if the sphericity assumption for ANOVA not met. Differences were considered statistically significant if $p<0.05$. Graphs indicate individual mouse data or mean and SEM.

REFERENCES CITED

Council., N.R. (2011). In Guide for the Care and Use of Laboratory Animals (Washington (DC): The National Academies Press).

Daigle, T.L., Madisen, L., Hage, T.A., Valley, M.T., Knoblich, U., Larsen, R.S., Takeno, M.M., Huang, L., Gu, H., Larsen, R.*, et al.* (2018). A Suite of Transgenic Driver and Reporter Mouse Lines with Enhanced Brain-Cell-Type Targeting and Functionality. Cell *174*, 465-480 e422.

Littlejohn, E.L., Espinoza, L., Lopez, M.M., Smith, B.N., and Boychuk, C.R. (2019). GABA(A) receptor currents in the dorsal motor nucleus of the vagus in females: influence of ovarian cycle and 5alpha-reductase inhibition. J Neurophysiol *122*, 2130-2141.

Schneider, C.A., Rasband, W.S., and Eliceiri, K.W. (2012). NIH Image to ImageJ: 25 years of image analysis. Nat Methods *9*, 671-675.

Strain, M.M., Espinoza, L., Fedorchak, S., Littlejohn, E.L., Andrade, M.A., Toney, G.M., and Boychuk, C.R. (2023). Early central cardiovagal dysfunction after high fat diet in a murine model. Sci Rep *13*, 6550.

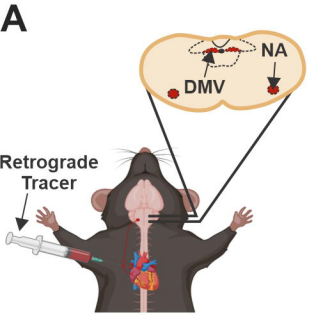
A
NA
DMV
Retrograde
Tracer

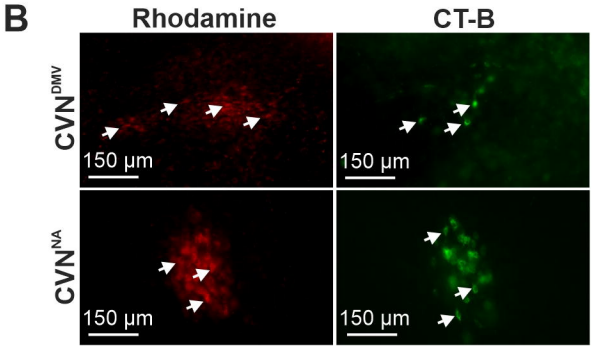
B
Rhodamine
CT-B
CVN^DMV
CVN^NA
150 µm
150 µm
150 µm
150 µm

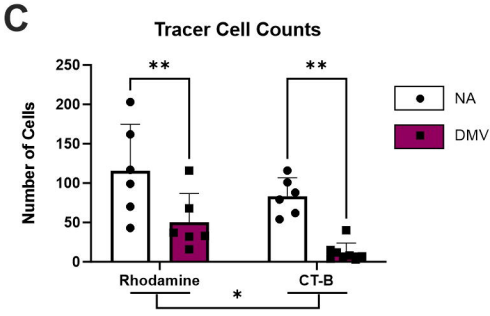
C
Tracer Cell Counts
Number of Cells
250
200
150
100
50
0
**
**
*
Rhodamine
CT-B
NA
DMV

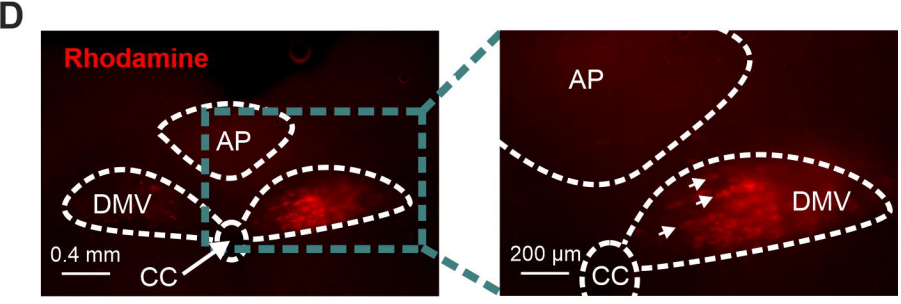
D
Rhodamine
AP
DMV
CC
0.4 mm
AP
DMV
CC
200 µm

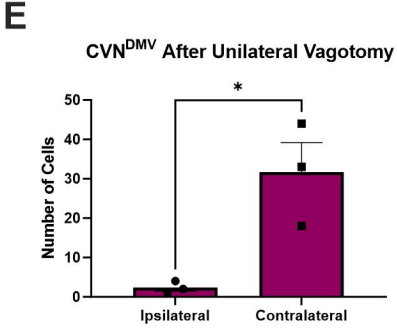
E
CVN^DMV After Unilateral Vagotomy
Number of Cells
50
40
30
20
10
0
*
Ipsilateral
Contralateral

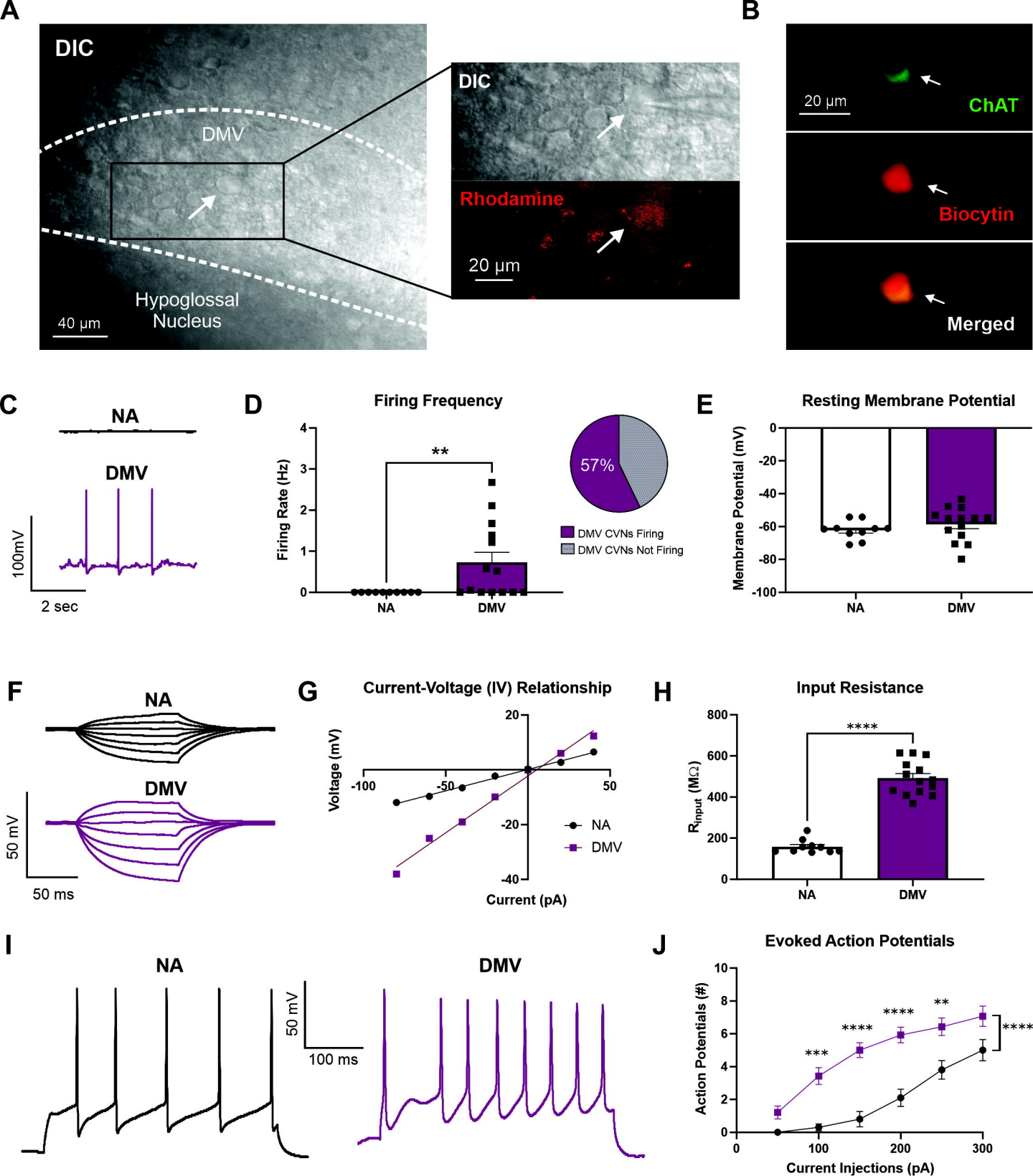
A
DIC
DMV
Hypoglossal Nucleus
40 µm
DIC
Rhodamine
20 µm
B
20 µm
ChAT
Biocytin
Merged
C
NA
DMV
100mV
2 sec
D
Firing Frequency
Firing Rate (Hz)
**
NA
DMV
57%
DMV CVNs Firing
DMV CVNs Not Firing
E
Resting Membrane Potential
Membrane Potential (mV)
NA
DMV
F
NA
DMV
50 mV
50 ms
G
Current-Voltage (IV) Relationship
Voltage (mV)
Current (pA)
NA
DMV
H
Input Resistance
R_input (MΩ)
****
NA
DMV
I
NA
DMV
50 mV
100 ms
J
Evoked Action Potentials
Action Potentials (#)
Current Injections (pA)
***
****
****
**
****

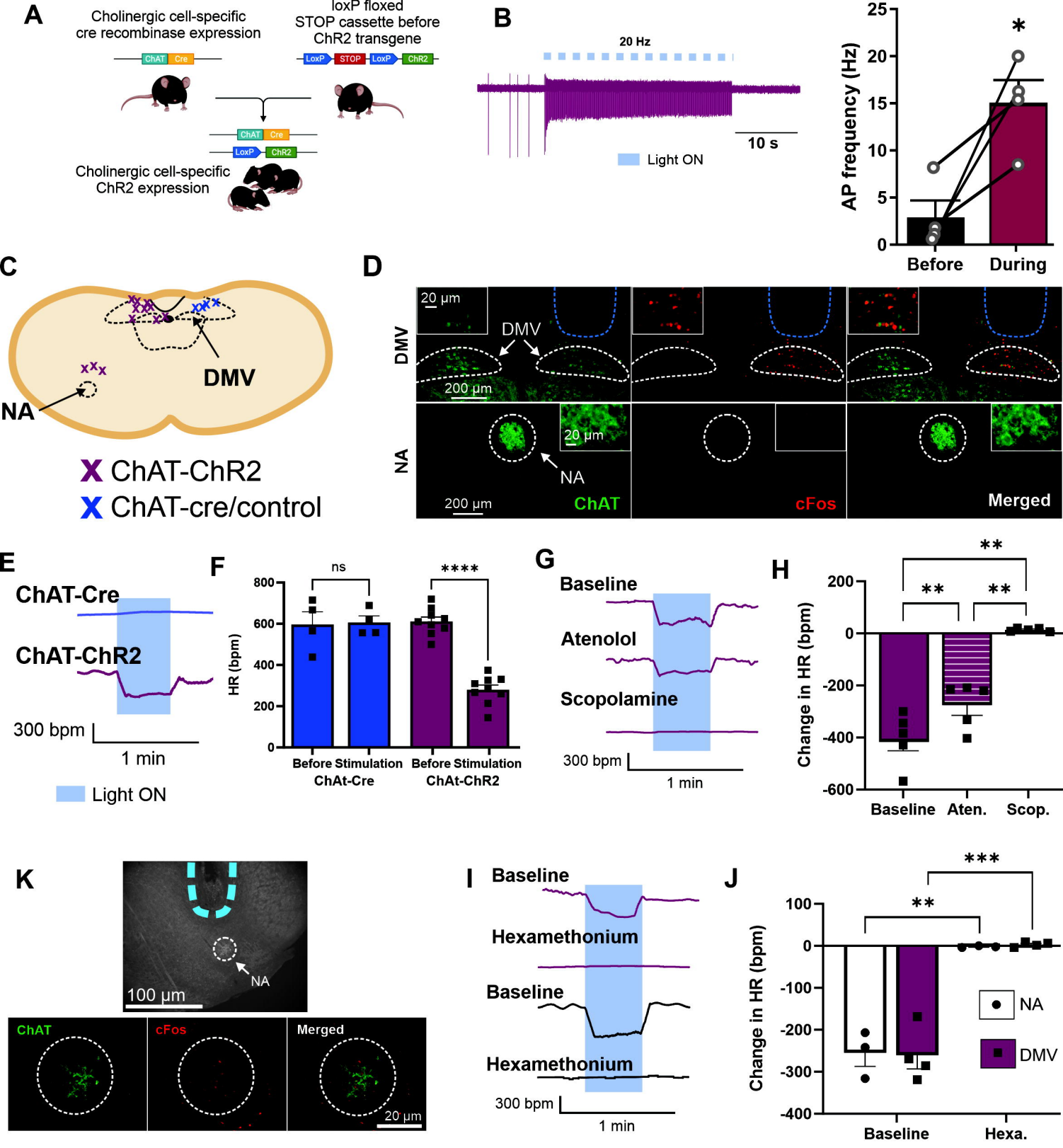
A
Cholinergic cell-specific cre recombinase expression
loxP floxed STOP cassette before ChR2 transgene
ChAT
Cre
LoxP
STOP
ChR2
Cholinergic cell-specific ChR2 expression
B
20 Hz
10 s
Light ON
AP frequency (Hz)
Before
During
C
DMV
NA
ChAT-ChR2
ChAT-cre/control
D
20 µm
DMV
200 µm
NA
ChAT
cFos
Merged
E
ChAT-Cre
ChAT-ChR2
300 bpm
1 min
Light ON
F
ns
****
HR (bpm)
Before Stimulation
ChAt-Cre
ChAt-ChR2
G
Baseline
Atenolol
Scopolamine
300 bpm
1 min
H
Change in HR (bpm)
Baseline
Aten.
Scop.
K
NA
100 µm
ChAT
cFos
Merged
20 µm
I
Baseline
Hexamethonium
Baseline
Hexamethonium
300 bpm
1 min
J
Change in HR (bpm)
NA
DMV
Baseline
Hexa.

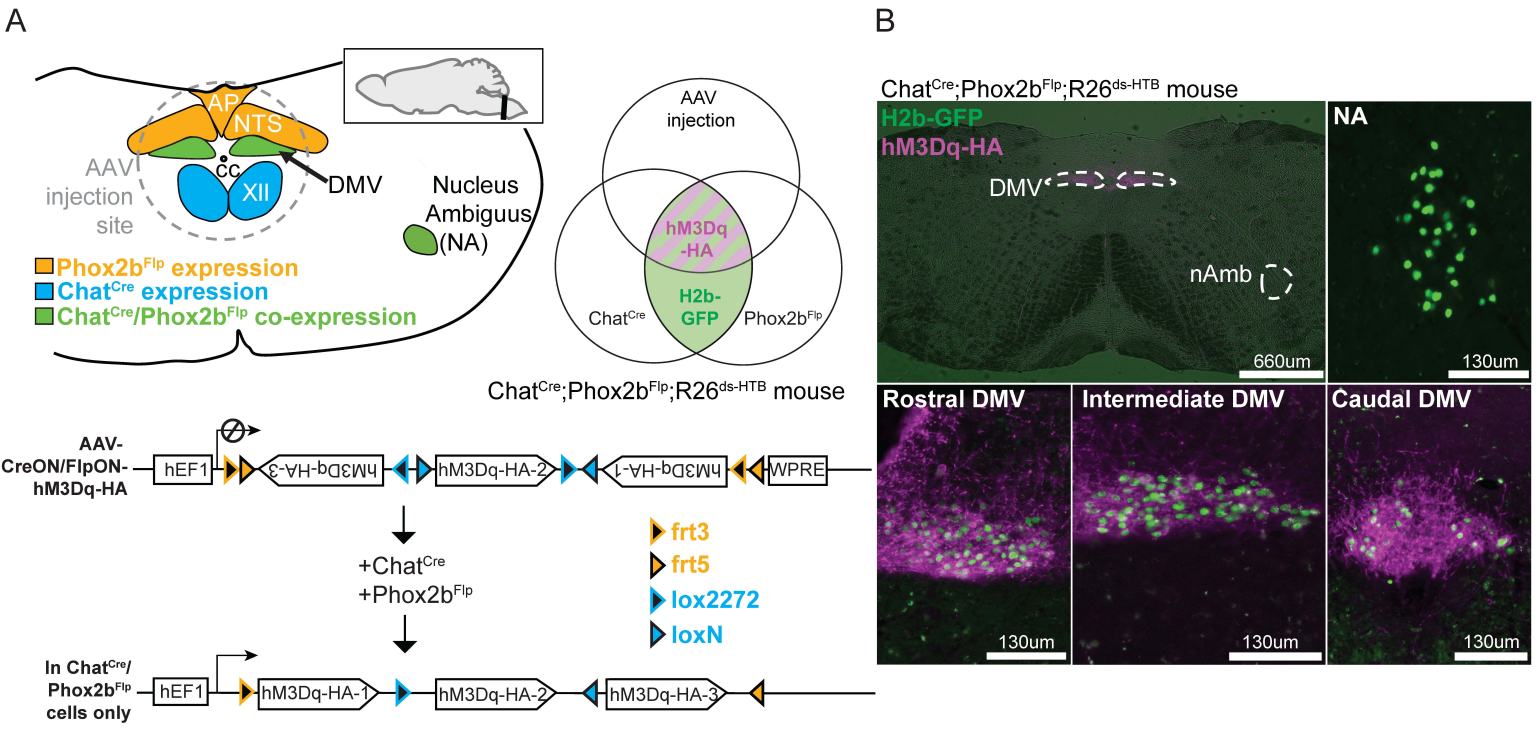
A
AP
NTS
AAV injection site
CC
XII
DMV
Nucleus Ambiguus (NA)
Phox2b^Flp expression
Chat^Cre expression
Chat^Cre/Phox2b^Flp co-expression
AAV injection
hM3Dq -HA
H2b-GFP
Chat^Cre
Phox2b^Flp
Chat^Cre;Phox2b^Flp;R26^ds-HTB mouse
AAV-CreON/FlpON-hM3Dq-HA
hEF1
hM3Dq-HA-3
hM3Dq-HA-2
hM3Dq-HA-1
WPRE
+Chat^Cre
+Phox2b^Flp
frt3
frt5
lox2272
loxN
In Chat^Cre/Phox2b^Flp cells only
hEF1
hM3Dq-HA-1
hM3Dq-HA-2
hM3Dq-HA-3
B
Chat^Cre;Phox2b^Flp;R26^ds-HTB mouse
H2b-GFP
hM3Dq-HA
DMV
nAmb
660um
NA
130um
Rostral DMV
Intermediate DMV
Caudal DMV
130um
130um
130um

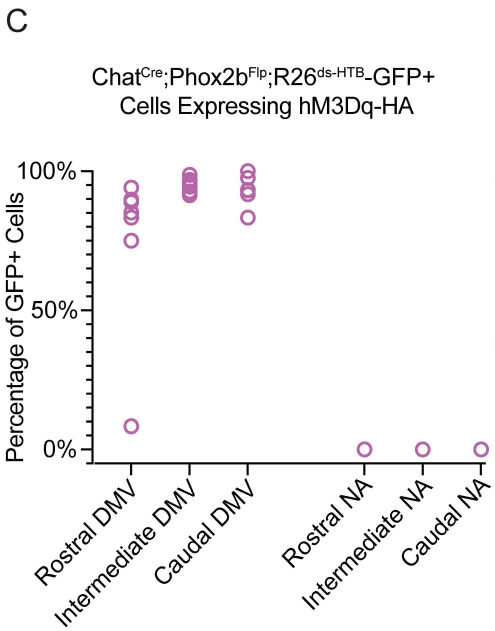
C
Chat^Cre;Phox2b^Flp;R26^ds-HTB-GFP+ Cells Expressing hM3Dq-HA
Percentage of GFP+ Cells
100%
50%
0%
Rostral DMV
Intermediate DMV
Caudal DMV
Rostral NA
Intermediate NA
Caudal NA

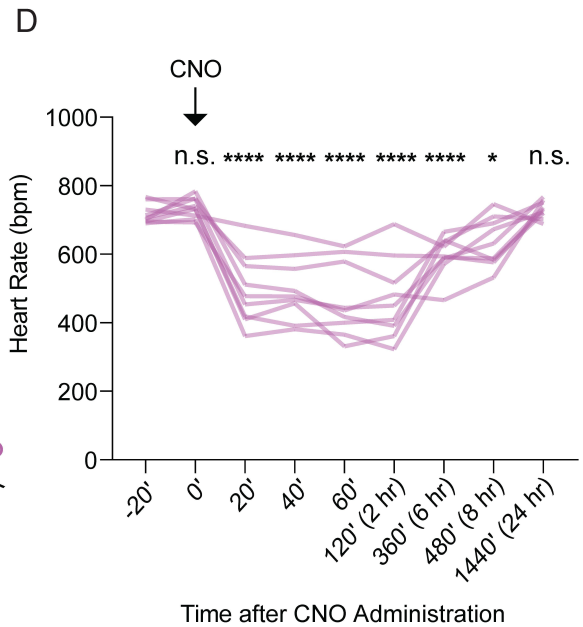
D
CNO
n.s. **** **** **** **** **** * n.s.
Heart Rate (bpm)
1000
800
600
400
200
0
-20'
0'
20'
40'
60'
120' (2 hr)
360' (6 hr)
480' (8 hr)
1440' (24 hr)
Time after CNO Administration

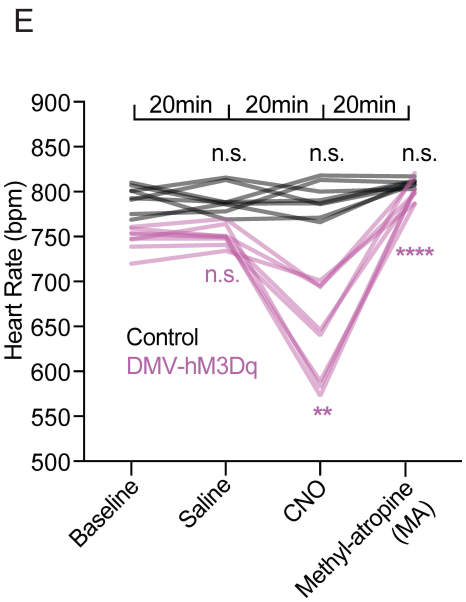
E
20min
20min
20min
n.s.
n.s.
n.s.
n.s.
****
**
Heart Rate (bpm)
900
850
800
750
700
650
600
550
500
Control
DMV-hM3Dq
Baseline
Saline
CNO
Methyl-atropine (MA)

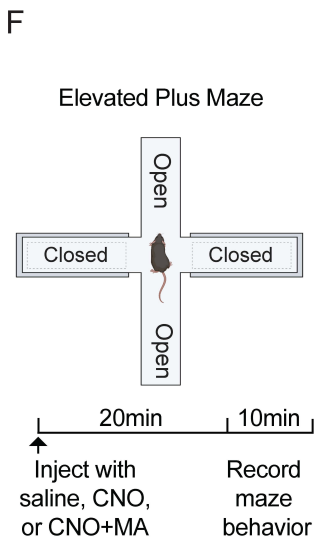
F
Elevated Plus Maze
Open
Closed
Closed
Open
20min
10min
Inject with saline, CNO, or CNO+MA
Record maze behavior

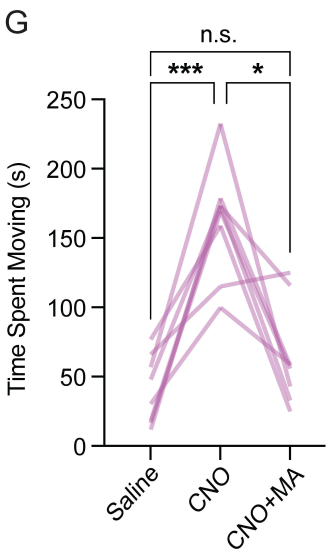
G
n.s.
***
*
Time Spent Moving (s)
250
200
150
100
50
0
Saline
CNO
CNO+MA

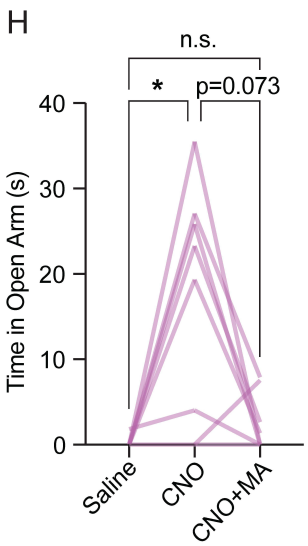
H
n.s.
*
p=0.073
Time in Open Arm (s)
40
30
20
10
0
Saline
CNO
CNO+MA

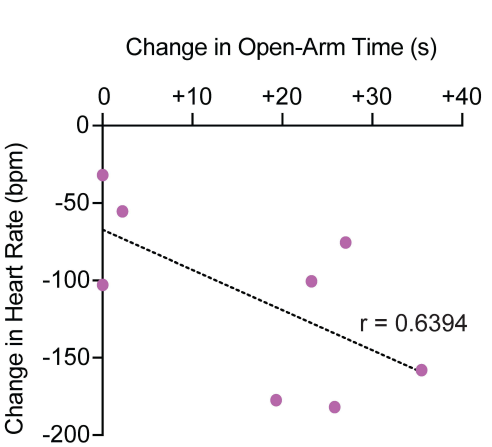
I
Change in Open-Arm Time (s)
0
+10
+20
+30
+40
Change in Heart Rate (bpm)
0
-50
-100
-150
-200
r = 0.6394

A

Chat^{Cre};Phox2b^{Flp};R26$^{ds\text{-}HTB}$ mouse

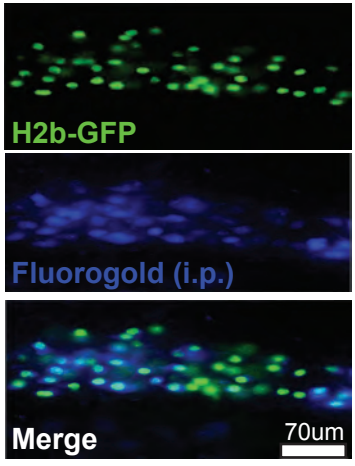

B

R26$^{ds\text{-}HTB}$ mouse (no Cre or Flp)

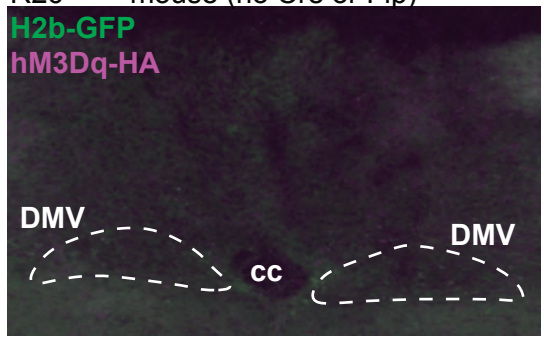

C

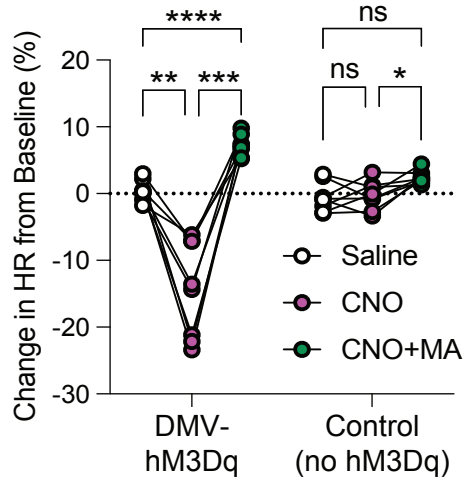

D

Control mice (no hM3Dq)

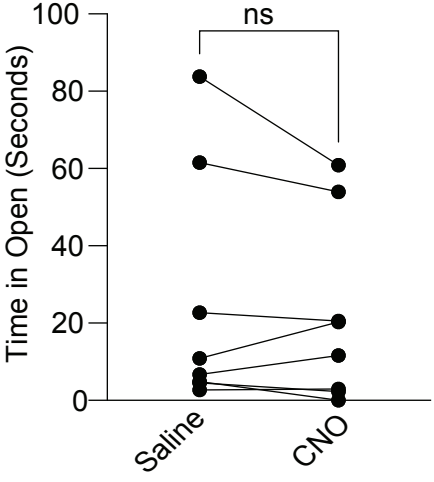

E

DMV-hM3Dq mice

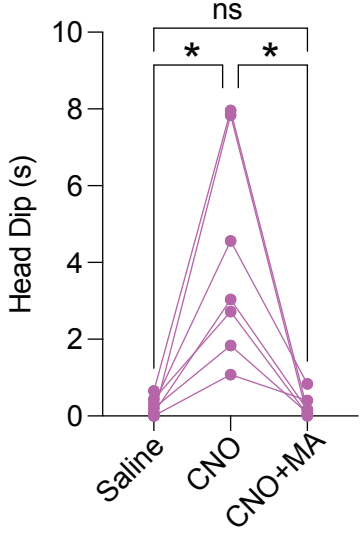

F
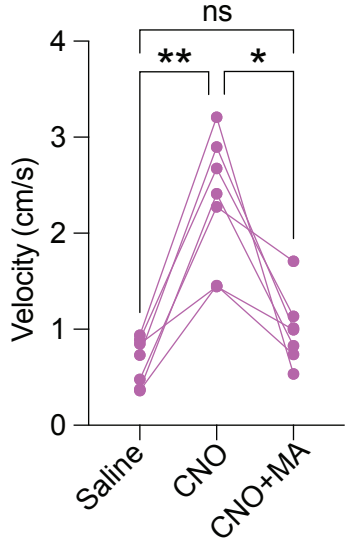
DMV-hM3Dq mice